U.PORTO

FACULDADE DE CIÊNCIAS
UNIVERSIDADE DO PORTO

MSc

2.º CICLO

FCUP
ANO

U.PORTO

Study of Polyvinylidene Fluoride in Fiber Optics sensing technology

António Vaz Rodrigues

FC

Study of Polyvinylidene Fluoride in Fiber Optics sensing technology

António Vaz Rodrigues

Dissertação de Mestrado apresentada à
Faculdade de Ciências da Universidade do Porto em
Engenharia Física

2016

U.PORTO

FACULDADE DE CIÊNCIAS
UNIVERSIDADE DO PORTO

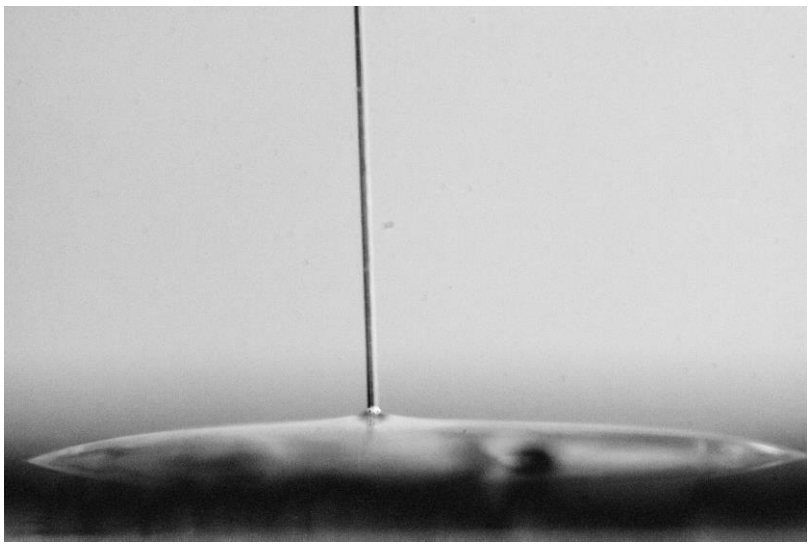

Study of Polyvinylidene Fluoride in Fiber Optics sensing technology

António Vaz Rodrigues
Integrated Master's in Engineering
Department of Physics and Astronomy
2016

Supervisor
Orlando José dos Reis Frazão, Invited Assistant Professor,
Faculty of Sciences of the University of Porto and
Senior Researcher, INESC TEC

Co-Supervisor
André Miguel Trindade Pereira, Assistant Professor,
Faculty of Sciences of the University of Porto

All modifications determined by the Jury, and only those, were made.

The president of the Jury

Porto, _____/_____/_____

Acknowledgements

This work is a milestone in my academic path. During this journey everyone who helped me is remembered. Some people have great importance, and I would like to thank them.

First, I would like to thanks my family, in special my mother, Manuela, who has been, and always will be, a strong pillar for all aspects of my life. Thanks for the support and advices that were given to me.

The most special thanks goes to Gonçalo, my boyfriend and all-time companion, thanks for being who you are, and always helping me keeping concentrated in my work and forcing the necessary breaks. Thanks for enduring the bad mood during stressful moments, that weren't so few.

To my supervisor, Dr. Orlando, and co-supervisor, Dr. André, for all the knowledge given and for all the guidance not only during this year, but during all the academic path so far.

To all my faculty friends and colleagues that began or joined this path alongside me, thanks for the moments and for the friendship that will be remembered. Thanks to my closest lab companions, Regina, Miguel and Catarina (my favorite bully), for all the days spent working and discussing our works together, always supporting each other's up. To Rui, that has also been a great companion and is an excellent student, for helping me keep committed with my work even in the worse moments. Also, thanks Pedro, for all the technical support.

Thanks to INESC-TEC and IFIMUP for providing me the tools and the place to work. Also, thanks to Requimte and CENTI for the help given to be able to perform important parts of the work. To the CORAL project, financed by FCT – Fundação para a Ciência e Tecnologia (Portuguese Foundation for Science and Technology) and by ERDF (European Regional Development Fund) through: COMPETE Programme (Operational Programme for Competitiveness) within project FCOMP-01-0124-FEDER-037281; ON.2 – O Novo Norte (Northern Portugal Regional Operational Programme).

Thanks also to those in Fluvial, Javardémica and CAUM for providing me my second families that are important for me.

Lastly, but not least, thanks to António Salcedo, who gave me my first laser pointer, which I still own today, for all the counseling that helped me understand my own direction.

Abstract

The work presented in this dissertation focuses in the importance of a low cost alternative to produce sensors, namely through the use of polymers such as Polyvinylidene Fluoride (PVDF), which was the chosen material for developing the work.

Polymers are very attractive in numerous applications as sensors, actuators and also biomedical applications, among others. Considering the fact that the Polyvinylidene Fluoride (PVDF) is a transparent polymer and is low-cost and easy to obtain at a larger scale, makes it an interesting material for optical applications. PVDF is also one of the most important polymers, and the first one to show ferroelectric properties due to its different crystalline phases. The β-phase has strong electroactive properties, comparable to those of conventional ceramic materials. Having the advantage of being low-cost and much more flexible that the ceramic materials.

The production of PVDF thin films in glass substrates and the coating of optical fibers with PVDF, as well as the identification of the obtained phases, which is vital for technological applications, are explored. Throughout the present work, the main used characterization techniques for this purpose are discussed (Fourier Transform Infrared Spectroscopy, X-ray Diffraction and Differential Scanning Calorimetry). The characterized samples show the presence of the most electroactive β-phase and the γ-phase.

The polymer is used to create optical devices based in interferometric principles. Different Fabry-Perot cavity configurations are studied by depositing thin films of PVDF in the cleaved end-face of single mode fibers (SMFs) and in the end-face of a hollow tube previously fusion spliced to the SMF. At the end, a proof-of-concept of a new device was tested for both humidity and temperature. In order to study the sensors' response, different temperature (from 20ºC to 80ºC) and humidity (between 20%RH and 80%RH) tests are performed. The characterized devices presented maximum sensitivities of 137 pm/K and 39.28 pm/%RH.

Keywords: Optical Fiber, Sensing Technology, Material Characterization, Polyvinylidene Fluoride, Fabry-Perot, Interferometry, X-Ray Diffraction, Fourier Transform in the Infrared Spectroscopy, Differential Scanning Calorimetry

Resumo

O trabalho desenvolvido ao longo desta dissertação foca-se na importância de alternativas de baixo-custo para produção de sensores, nomeadamente através da utilização de polímeros como o Fluoreto de Polivinilideno (PVDF), que é o material escolhido para o trabalho.

Os polímeros são materiais interessantes para desenvolver sensores e atuadores, mas também para ser utilizado em aplicações médicas, como imagiologia, entre outras. Considerando que o PVDF é um polímero transparente e, sendo de baixo custo, é fácil de obter a uma maior escala, faz dele um material interessante para aplicações óticas. O PVDF é também um dos polímeros mais importantes, sendo o primeiro a demonstrar propriedades ferroelétricas originadas nas suas diferentes fases cristalinas. A fase β tem propriedades eletroativas fortes, comparáveis com as de materiais cerâmicos convencionais, tento a vantagem de ser de baixo custo e muito mais flexível que os anteriores.

A produção de filmes finos de PVDF em substratos de vidro e o revestimento de fibras óticas com PVDF são explorados, assim como a identificação das fases de PVDF obtidas, que é importante para a sua aplicação futura. Ao longo deste trabalho as principais técnicas de caracterização usualmente utilizadas são discutidas (Difração de Raios-X, Espetroscopia no Infravermelho por Transformada de Fourier, Calorimetria Diferencial de Varrimento). As amostras obtidas revelam a existência das fases β e γ.

O PVDF é usado para o desenvolvimento de dispositivos em fibra ótica usando princípios de interferência ótica. São desenvolvidas e estudadas diferentes configurações de cavidades de Fabry-Perot depositando o polímero na ponta cortada de uma fibra ótica convencional ou de uma fibra oca previamente unida à fibra ótica convencional. Por fim, uma prova de conceito de um novo dispositivo é sujeita a testes de caracterização, tanto em temperatura (de 20ºC a 80ºC) como humidade (entre 20%HR e 80%HR). Os dispositivos apresentaram sensibilidades máximas de 137 pm/K e 39.28 pm/%RH.

Palavras-Chave: Fibra Ótica, Tecnologia Sensora, Caracterização de Materiais, Fluoreto de Polivinilideno, Fabry-Perot, Interferometria, Difração de Raios-X, Espetroscopia no Infravermelho por Transformada de Fourier, Calorimetria Diferencial de Varrimento

Contents

List of Figures

List of Tables

Nomenclature

DMF - Dimethylformamide

DSC – Differential Scanning Calorimetry

FP – Fabry-Perot

FTIR – Fourier Transform Infrared Spectroscopy

FTIR-ATR – FTIR using Attenuated Total Reflection

FWHM - Full Width at Half Maximum

GPIB – General Purpose Interface Bus

IEEE-488 - GPIB

IR – Infrared

ITO – Indium Tin Oxide

LASER - Light Amplification by Stimulated Emission of Radiation

LMR - Lossy Mode Resonance

OSA – Optical Spectrum Analyzer

PVDF – Polyvinylidene Fluoride

PVDF/DMF – PVDF dissolved in DMF

SMF – Single Mode Fiber

VI – Virtual Instrument

XRD – X-ray diffraction

1 Introduction

1.1 Motivation

During the last decades, polymer technology has been continuously investigated and has proven being capable of having applications in various areas as sensors, actuators, field-effect transistors or information storage due to their ferroelectric nature [1].

The low value of acoustic impedance of polymers has drawn the attention of researchers, because it allows the acoustic matching between polymers and water, making them suitable to applications as hydrophones and medical ultrasound imaging [2]. Polymers also have the advantage of being cheap and easy to produce, which are nuclear factors in the industry. Due to their flexibility, they also have the possibility of being applied to complex geometries and are more durable where deformable materials are needed [3].

Polyvinylidene fluoride (PVDF) is among the set of polymers which present piezoelectric, pyroelectric or ferroelectric properties, and since its piezoelectric nature discovery in 1969 [2] a wide range of applications have been researched until today. PVDF composites have been produced leading to a larger range of applications based, for example, in the magnetoelectric effect [2–4].

Although the piezoelectric coefficient of PVDF is comparable to those of ceramic materials, the piezoelectricity is not always present in the polymer. The β-phase of PVDF has the highest dipole moment per unit cell among all PVDF crystalline configurations due to the high electronegativity of the Fluor atoms in the unit cell. This is the reason why this phase is the most interesting for the applications mentioned [5].

Obtaining a PVDF sample in the purest β-phase is a complex task, many methodologies for the production of this electroactive phase have been studied. Most of the methodologies cannot produce 100% pure β phase, depending on the application purpose and geometry, different methodologies such as solvent casting, thin film stretching or electrospinning are used to produce PVDF membranes, thin-films or nano-fibers [4].

Some of the most important areas of application of PVDF are acoustic sensing where different kinds of microphones and hydrophones have been designed. This area is also related to ultrasound imaging, which is used in medicine, since the human body

is mostly composed by water. Other sensing elements, as thermometers or pressure gauges, have been developed [4]. Optical-based sensing using PVDF is also an interesting topic once it has a refraction index of 1.42, comparable to those of the optical fibers (n=1.44) [6].

The application of PVDF in fiber optic technology is addressed during the development of the thesis. As mentioned before, the piezoelectric nature of β-PVDF is interesting for possible applications in electrical current sensing [7]. In this case, the bound between the optical fiber and the polymer needed to produce the optical device needs special attention.

1.2 Objectives

- Obtention of the β phase of PVDF in a simple, low-cost and efficient method:
    - Explore the solvent casting method of PVDF to the optical fibers;
    - Characterization of PVDF samples using the main techniques referred in the literature (DSC, XRD and FTIR);
- Attaining a bound between the PVDF and the optical fiber;
    - Develop an optical sensor using PVDF as a sensing element;
    - Benchmark tests of the fabricated optical sensor;
- Implementing an electric field interferometric sensor based in optical fiber Fabry-Perot using PVDF as a transducer;

1.3 Outline

The first chapter has the intuit of presenting the purpose of the work's subject as well as presenting the main objectives that are pursued. The chapter also contains the structure of the document, as well as a brief enumeration of outputs due to the developed work.

The second chapter contains a brief introduction regarding the production of the desired PVDF phase. A state-of-the-art is also present in the chapter, the main applications of the PVDF in the sensing area are introduced.

The third chapter is focused in the analysis of the PVDF using the following three material characterization techniques; Differential Scanning Calorimetry (DSC); X-ray Diffraction (XRD); and Fourier Transform Infrared Spectroscopy using attenuated total reflection (FTIR-ATR). The deposition of the PVDF is studied both for thin films over silica substrates and for standard single mode fibers. The data of the techniques used for characterization are compared and a reliability/simplicity analysis is made.

In the fourth chapter, the optical properties of the PVDF/fiber bound are explored. The method of production of the bound, via dip coating technique is explained. A Fabry-Perot cavity formed using the PVDF is presented. The device is subjected to different tests. Both temperature and humidity tests are run using the device, and its response is presented and discussed.

The fifth, and final chapter is used to overview the previous chapters. A general discussion related to the work is presented followed by some final remarks and future work proposal.

1.4 Outputs

Communications in National/International Conferences

A. Vaz Rodrigues, O. Frazão, A. Trindade, PVDF deposition in optical fibers (in portuguese), Física 2016 - 20a Conferência Nacional de Física, Braga, Portugal, September, 2016.

A. Vaz Rodrigues, A. Pereira, O. Frazão, *Fabry-Perot cavity using Polyvinyldene Fluoride (PVDF)*, SEONs 2016 - XIII Symposium on Enabling Optical Networks and Sensors, vol.1, no.1, pp.2, Covilhã, Portugal, July, 2016.

A. Vaz Rodrigues, O. Frazão, A. Trindade, *PVDF based fiber optic sensors*, JEFFE 2016 - Jornadas de Engenharia Física e Física Experimental 2016, Porto, Portugal, February, 2016.

2 State of the art

The interest in PVDF-based technologies in photonics is essentially due to its potential as a transducer. Currently PVDF has already been deeply studied in different fields of physics, resulting in the use of PVDF in applications such as touch screens, ferroelectric devices, power conversion, among others. These technologies are essentially based on the electrical response of the polymer to a mechanical stimulus, the piezoelectric effect. However, PVDF also shows the opposite effect to the piezoelectric effect, that is, this polymer is also able to respond to an electrical stimulus in order to produce a mechanical deformation.

This work is focused on the optical based applications of PVDF as an optical sensor and transducer, but applications of PVDF are extended to areas as tactile sensors, ferroelectric devices, energy conversion devices, shock sensor, thermal measurement devices, pyroelectric infrared arrays, dust sensors, batteries, filters, chemical protection, and magnetic field sensors [2,4,8]

2.1 PVDF obtention and characterization techniques

The PVDF's monomer is composed by Fluor, Carbon, and Hydrogen, two atoms each. Through the polymerization process, depicted in the Figure 2.1, monomers can be linked in different ways within a PVDF polymer chain.

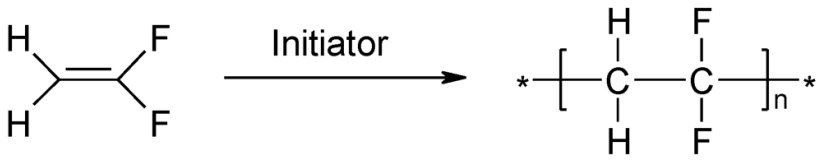

Figure 2.1 - Polymerization of the VDF monomer into PVDF

The various pairs of Fluor atoms can be positioned in the same side of the chain, producing a stronger dipole moment in the chain, or they can be arranged in order to cancel out this configuration, as can be seen in the Figure 2.2. The different crystal structures of PVDF allows it to have different mechanical and electromagnetic properties. In terms of electromagnetic properties, PVDF in the β phase has the largest piezoelectric coefficient compared to other synthetic polymers, as well as also having other properties, such as pyroelectricity, and nonlinear optical properties [5].

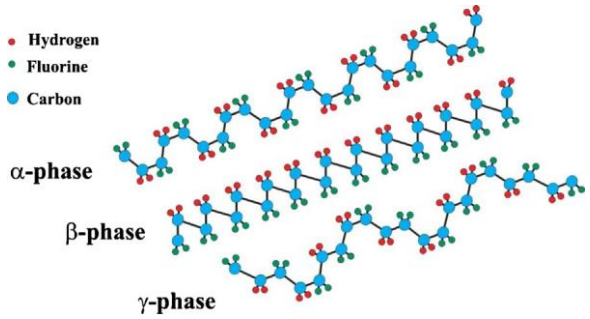

Figure 2.2 - Representation of PVDF chains for different phases [4]

PVDF in the β-phase is the most required phase, even having a simple structure, it is complex to obtain a sample with high β-phase purity. Martins et al. [4] has done an excellent revision on the most used methodologies to obtain the β-phase as well as the characterization techniques used for phase identification. This electroactive phase can be obtained from a variety of methods starting from the PVDF melt, the α phase or a PVDF solution. It is also possible to form β-like electroactive phases producing PVDF copolymers, or using materials as fillers, which will serve as a catalyst element. Some of the methodologies generally used to transform PVDF between different phases are condensed in the phase diagram of the Figure 2.3 [5].

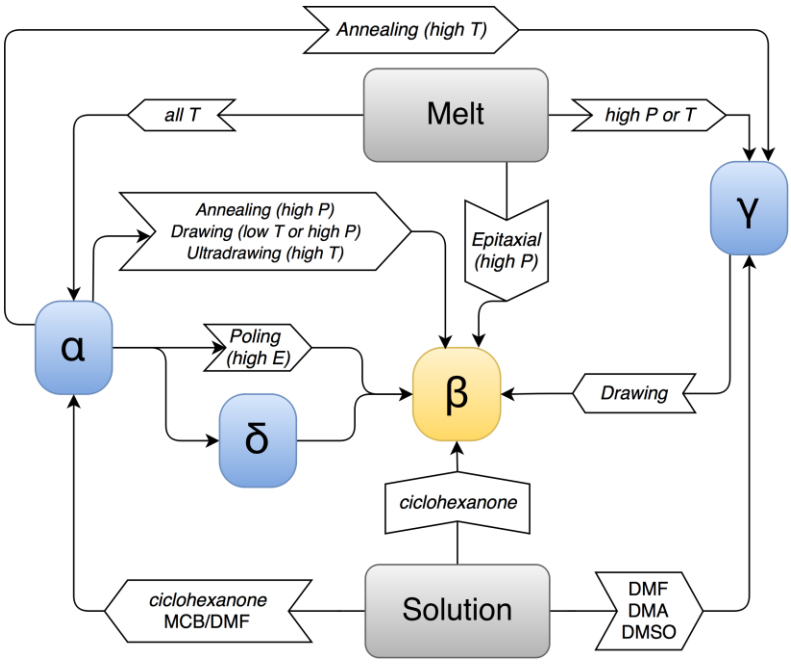

Figure 2.3 - PVDF phase transformations (adapted from [5])

One of the ways to obtain the electroactive PVDF is solvent casting. PVDF can be dissolved in various solvents as N,N-dimethylformamide (DMF) or acetone. For example, starting from a solution of PVDF, the Electrospinning technique, which relies on the use

of high electric fields, produces sub-micron to nano-scale fibers of PVDF. Also starting from a PVDF solution, spin-coating is an alternative to evaporative deposition to coat higly-polished substrates. If a poled β-PVDF ultrathin film is desired, the Langmuir-Blogett technique is a suitable method because it doesn't need a poling treatment. If the PVDF solvent used is DMF or dimethyl acetamide, a simple crystallization of PVDF from the solution below T = 70 ºC shows a pure β-phase. A drawback of this processes is the high degree of porosity of the polymer which is very fragile, degrades electrical properties, and doesn't allow the poling treatment. However, porosity can be eliminated by applying pressure perpendicular to the film at high temperatures (140 - 160 ºC). After this process, the film possesses high flexibility and is transparent to visible light [4].

Transformation to the β phase can be further enhanced by associating the Corona effect. This effect consists in applying a voltage difference high enough to create an electrical discharge between two electrodes separated in air, this discharge will pole the PVDF [4].

In order to characterize the obtained PVDF phase some techniques are reported in the literature and are recurrently used by the majority of the researchers. The first PVDF phases, α and β, have been identified using techniques as FTIR and XRD. But when the γ-phase was discovered, it was sometimes mistaken with the β-phase. A correct identification of the phase is possible to cross-analyzing the results of the techniques mentioned above and DSC. Otherwise, a careful interpretation of each technique is needed [4].

The FTIR technique is a non-destructive technique which allows the identification of the different phases of PVDF as α, β and γ through the identification of the vibrational bands of each phase. This technique is primarily used for a qualitative evaluation of the different phases, but in some special cases, a quantitative analysis can be performed [4]. It can be seen that some absorption bands from the β and γ phases are overlapped, essentially in the 840 cm^{-1} band, see Figure 2.4, where the overall absorption band for the γ-phase is broader, due to the existence of an absorption band at 833 cm^{-1}. The α-phase has other characteristic absorption bands that do not overlap with those of the other phases, making this phase easily detectable [4].

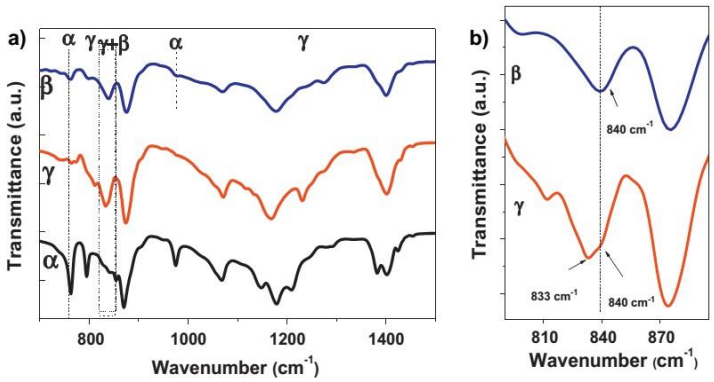

Figure 2.4 - FTIR Transmitance spectra for diferent phases [4]

PVDF phase identification is also possible with XRD analysis, where is possible to analyze the crystal/molecular structure. In the XRD diffraction analysis, there can be some confusion in the identification between α and γ phases because the diffraction angle for the (110) plane of α is almost the same as for the (002) and (110) planes of γ. Even if the characteristic peak near 27º for the α is not present, in the case of the shoulder for the (020) plane is not noticeable, doubts may arise between the β and γ phases. These characteristic spectra can be seen in Figure 2.5 [4].

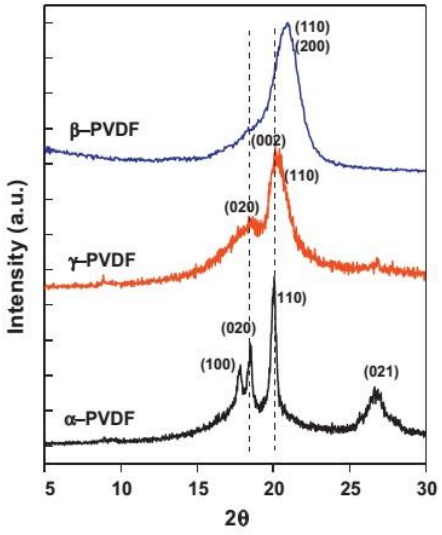

Figure 2.5 - XRD curves for diferent phases [4]

The DSC analysis is typically used as a complement for the aforementioned structural techniques. In the DSC analysis, the different melting temperatures are analyzed for each phase. The melting temperature depends not only on the crystalline phase but also on the sample's morphology, size and quantity of defects. As β and α phases have a similar melting temperature (around 167 – 172ºC), this technique is not used to distinguish between these two phases (see Figure 2.6). When phase γ is present, the melting temperature is around 179 – 180ºC. This allows the identification of the presence of this phase [4].

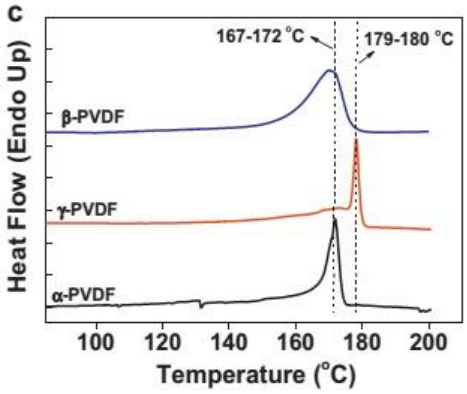

Figure 2.6 - DSC typical curves for differnt PVDF phases [4]

2.2 Electrical-based Sensors

An electrical sensor is based on the electrical response of the sensor mechanism to different inputs, as mechanical or temperature variation in the case of piezoelectric and pyroelectric materials [4]. As a piezo-material, the response to a mechanical input is an electrical one, hence, PVDF can be used as a transducer to serve as an acoustic sensor (hydrophone, microphone) [9,10], gas pressure [11], and tactile sensors [4]. PDVF is also a pyroelectric material, which means that it produces an electrical response to a temperature variation allowing the implementation of temperature sensors for cryogenic measurements [12], near room temperature measurements [13], and energy sensors for optical radiation [14]. Recently, based in the piezoresistive nature of a PVDF composite, highly sensitive tactile devices have been developed [15].

2.2.1 Acoustic and Pressure sensors

PVDF electrical response was turned to a low-cost acoustic sensor by manufacturing a needle or a membrane, see Figure 2.7. Both sensors have attached electrodes to pick-up the electrical signal due to the piezoelectric response [9,10].

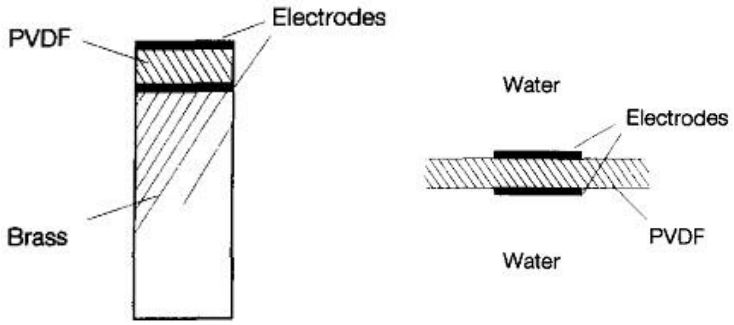

Figure 2.7 - Acoustic sensor configurations: needle [9] (left) and membrane [10] (right)

The two hydrophones have a working frequency range that spans from 1 MHz to 25 MHz and have sensibilities of 55 mV/Pa for the 0.2 mm needle hydrophone from Precision Acoustics [16] and of 61 mV/Pa for the membrane hydrophone from the literature [10].

A pressure sensor was also developed using the same principle as the acoustic sensors. In the Figure 2.8, a schematic (left) and response of this pressure sensor (right) are represented. This sensor can be used for many cycles without losing efficiency as long as the pressure is below 100 kPa. The device's temperature dependent sensitivity ranges between ~ 2 mV/Pa at -25 ºC and ~7 mV/Pa at 65 ºC, but the sensor's working temperatures span from -25 ºC to 160 ºC. The sensitivity is also humidity dependent but does not vary as much compared to the temperature dependence [11].

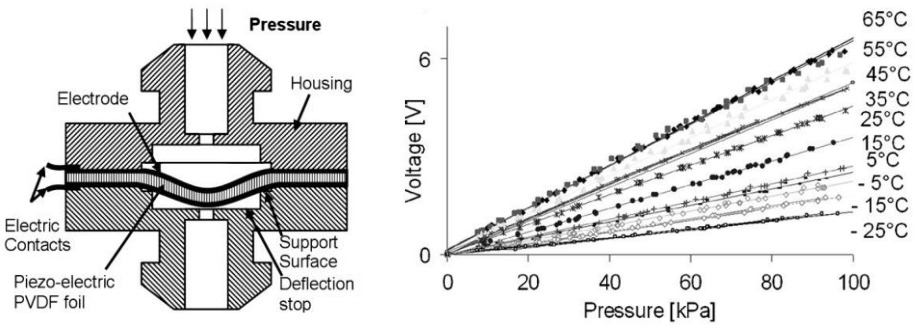

Figure 2.8 - PVDF pressure sensor design and response [11]

2.3 Optical-based Sensors

An optical sensor relies essentially on the mechanical response of the device to different kinds of inputs. In the case of piezoelectric materials, the material can be used as a transducer. If used together with an interferometric optical sensor, the mechanical response of the material is used as an input to the optical sensor. In a piezoelectric material the response to an electrical input is a mechanical one. This way, PVDF can be used as a low cost transducer to serve as an electric field sensor [7].

2.3.1 Electric field sensors

A strip of PVDF can be used to induce stress in an optical fiber if jacketed to it. These strains induce a phase change because the optical path is changed. Using an interferometer as a Mach-Zehnder (see Figure 2.9), the relative phase difference can be measured [7].

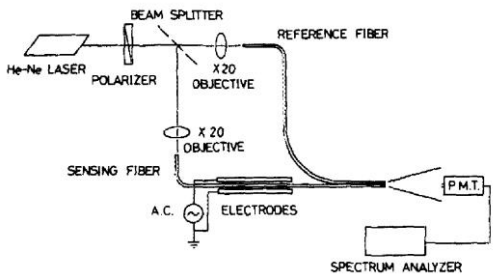

Figure 2.9 - Mach-Zehnder interferometer for Electric field sensing [7]

The phase changes for this kind of sensor have been measured in terms of field intensity and frequency and are presented in the Figure 2.10. In this sensor, the PVDF is used as a transducer from electric field to mechanical strain actuator. For a 800 Hz frequency input, the measured sensitivity was 1.5×10^{-7} rad/(V.m^{-1})/m but the maximum sensitivity exceeding 10^{-5} rad/(V.m^{-1})/m was verified for low frequency fields around 35 Hz [7].

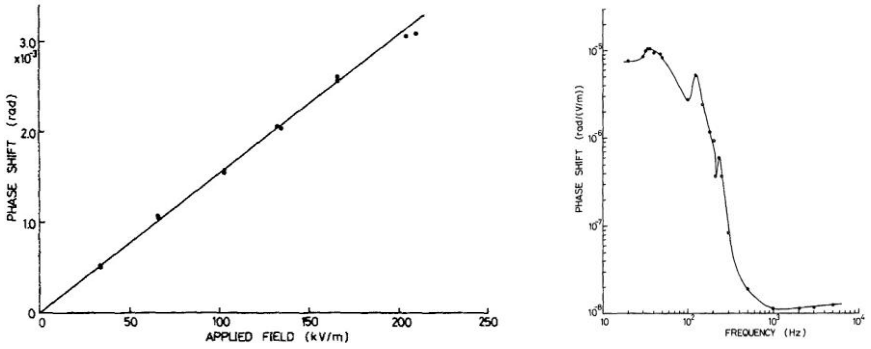

Figure 2.10 - Induced phase chage for electric field intensity (left) and frequency (right) [7]

This same setup of the sensor can also be used as an actuator, if used as phase shifting element or modulator, this is, the applications of this jacketed optical fiber are not restricted to sensor applications [7].

Another current sensing device has recently been reported in the literature. This sensor principle was based in Lossy Mode Resonances (LMRs) where an inner electrode composed of Indium Titanium Oxide (ITO) was deposited onto a 200 μm core multimode optical fiber, over this ITO layer, a PVDF thin film was deposited, and finally another ITO layer, the outer electrode [17]. PVDF was chosen as the sensing element due to the device's production cost being greatly reduced. The reported sensitivity for this device is of 1 nm/V for voltages above 80 Volts [18].

2.3.2 Humidity sensor

An intensity optical sensor linked to electrospun PVDF nanowebs in a hollow core section of an optical fiber (see Figure 2.11) was used to develop a highly sensitive humidity sensor, 0.05 dB/%RH in the 40-70 %RH range, with a fast response (100 ms rise time) for human breathing monitoring [19]. A similar sensor was proposed using polymer optical fiber instead of the hollow tube [20].

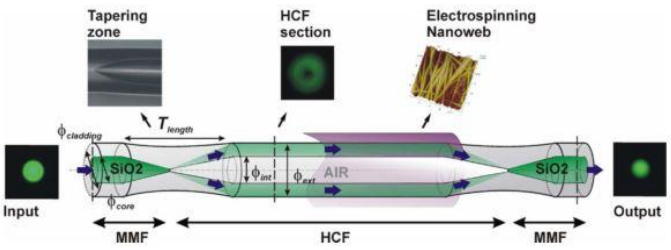

Figure 2.11 - Scheme of a humidity sensor [19]

2.4 Concluding Remarks

In this chapter, some of the important aspects that make PVDF interesting for sensing applications are revised. Knowing that the PVDF can exist in different crystalline phases is of the greatest importance, because some applications need electroactive materials in order to work. This way, the importance of obtaining the β-phase was explained. The methods to obtain the most electroactive were also briefly presented, and used to choose a β-phase production methodology.

The main characterizations techniques for the PVDF that are found in the literature were presented. The important details for identifying the different phases of PVDF were explained for the three techniques: DSC, XRD, and FTIR.

Important applications of PVDF as a sensing element were presented for electrical based sensors. The recent investigation of the application of PVDF as versatile, simple and low cost option in optical sensing technology is revised.

3 PVDF characterization

3.1 Introduction

As mentioned in the introduction the Polyvinylidene Fluoride (PVDF) is a polymer which can present several crystallographic phases where the different types of phases in which the PVDF can exist is determined by the organization of its chains, either within the chains, or among several chains.

Two distinct samples of PVDF may appear equal at the naked eye but may present different PVDF phases. In order to characterize the samples and identify the phases of PVDF several techniques such as X-ray diffraction (XRD), Fourier Transform Infrared Spectroscopy (FTIR), or Differential Scanning Calorimetry (DSC) can be employed.

In the X-ray diffraction technique, the sample is tested in terms of crystallographic properties. The polymer is not a well-organized crystal, but the spatial configuration of the chains in some of the phases has the same properties as crystalline structures (periodicity). Running a XRD measurement to the sample may determine the crystallinity of the PVDF and help narrow down the possible phases, if not the present phase of the PVDF in the sample. The characterization was performed at the ambient temperature using a D5000 Siemens diffractometer in the Bragg Brentano configuration (θ-2θ), equipped with a copper anode X-ray source.

The Fourier Transform Infrared Spectroscopy analyses the IR absorption bands of the sample. This technique allows the user to obtain information concerning the different vibrational states of the bounds, internal and external to the polymer chains, allowing to distinguish and, in some cases, quantify them. In the case of PVDF, the different phases have different spatial configurations and the vibrational energies are also different. Though some phases have similar vibrational energies, some phases have a group of vibrational states that are like a fingerprint and provide a unique phase identification. The equipment used for the analysis is a PerkinElmer Spectrum BX FTIR System spectrophotometer equipped with a DTGS detector and a PIKE Technologies Gladi ATR accessory from 4000 to 400 cm^{-1} from the faculty's associate laboratory Requimte.

Differential Scanning Calorimetry provides information related to state transitions examining the heat flow of the endothermal and exothermal transitions. The technique can be used to determine the fusion and solidification temperature. The different phases of PVDF have different binding energies, and also different fusion energies. Subjecting a PVDF sample to this analysis will possibly and irreversibly alter the sample's phase

after the fusion point. When lowering the temperature below the solidification temperature will give rise to a different phase, depending on the conditions. A Perkin-Elmer DSC-7 differential scanning calorimeter is used to perform the measurements.

The three techniques' results can be compared and used to identify the PVDF phase. The XRD and FTIR are non-destructive techniques, and may be used in the same sample. Although it may help to correctly identify the present phase, the DSC is a destructive technique. If the PVDF is melted, all the crystalline phases of the PVDF disappear. After the cooling process the polymer may settle in a different phase than the initial one. This way, if the sample integrity is to be maintained or other characterization technique is to be used, the DSC analysis should be used with caution.

In this chapter, it was performed a thorough analysis and characterized by the three above mentioned methods. In this study, two kinds of samples were used, the first type is thin films of PVDF deposited over Silica substrates, and the second type of sample is formed by PVDF coating Single Mode Optical Fibers (SMF). The preparation methods for the samples, and for the solution of PVDF/DMF used to coat the samples are explained throughout the chapter.

3.2 PVDF/DMF Solution Preparation

In order to deposit the PVDF in the surface of the optical fiber and over the silica substrates, the dip coating method was used due to its simplicity and fast preparation method.

As N,N-Dimethylformamide (DMF) is a solvent of the PVDF polymer, a solution of PVDF/DMF is a possible starting point for the dip coating method to be implemented. After the evaporation of the DMF, the settled PVDF will return to its solid state. It is also known that the achievement of PVDF in the β-phase is possible using the PVDF/DMF solution. From literature, the drying process of the PVDF/DMF solution at relative high temperatures, above 70ºC, reduces the amount of the β-phase in the sample [21–23].

The solution was prepared by first pouring 10 mL of DMF into a flask. Prior to the addition of the DMF, a magnetic mixer was placed inside the container which was placed over a stirring hotplate. The temperature of the hotplate was set to 40 ºC. After pouring the DMF, a previously weighted PVDF powder was added to the flask, which was then sealed off with parafilm tape to prevent the DMF vapors to escape. The magnet stirrer was set to 700 rpm for about two hours to dissolve the powder into the DMF. The end result was the PVDF/DMF solution used for the dip process to be done. The complete PVDF/DMF preparation protocol can be found in the page 53.

Figure 3.1 - Stirring/Heating Setup for PVDF/DMF preparation

3.2.1 Thin films Preparation

The method used to coat the silica substrates is the dip coating method, where the substrate is submerged in a PVDF/DMF solution of 20 %wt concentration. Before coating the substrates, the solution was heated to 50ºC and stirred with the magnetic stirrer to maintain the uniformity of the mixture. The substrates were submerged for 10 seconds

with the help of tweezers. In the samples that were dipped two times, a period of 50 seconds separated each dip.

The substrates were then left to dry off the DMF to produce the PVDF film. The films that dried at 70 ºC were taken to an oven set to the desired temperature. The ones that were dried at ambient temperature were placed inside a fume hood. All the films were dried for 2 hours before being stored to be analyzed. The main information about the preparation of the thin films is resumed in the Table 3-I.

Sample	Dip time (s)	Dip Interval (s)	Drying temperature (ºC)	Drying time (h)
TF25_1	10 (x1)	50	25	2
TF25_2	10 (x2)	50	25	2
TF70_1	10 (x1)	50	80	2
TF70_2	10 (x2)	50	80	2

Table 3-I - Number of dips and drying time for thin films

3.2.2 Optical Fibers Coating

The method for coating the optical fibers is similar to what has been done for producing the thin films. The cladding of the SMF was first removed with a stripper, the exposed fiber was cleaved in order to have a uniform cut in the tip the fiber. The fiber was then dip coated in the PVDF/DMF solution. In the dip coating process, the length of fiber that was submerged was enough to coat both the tip and the side part of the exposed SMF.

Unlike what was done for the thin films, all the fibers were dipped only once. Each time that the fiber was submerged, the already coated area was again dissolved completely in the solution, thus, a second dip would work like a unique dip.

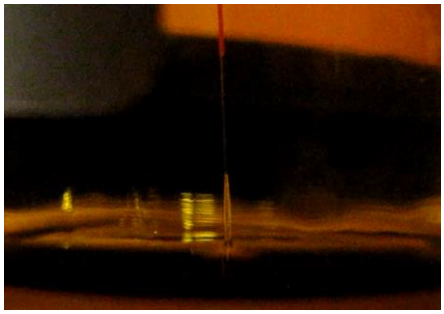

Figure 3.2 - Optical Fiber dip coating in PVDF/DMF solution

3.3 Differential Scanning Calorimetry (DSC)

The first technique used was the Differential Scanning Calorimetry where the heat flow to a sample in a pan is monitored. In order to be able to access the information of the sample, a reference curve is needed. The first performed measurement was the reference curve where two pans with only air inside where used.

In order to be able to measure the PVDF of the thin films, the polymer was removed from the substrate's surface, weighted in a precision balance and put in a pan which was then sealed. In the case of the optical fibers, it is difficult to remove the PVDF without breaking the optical fiber. The section of fiber is also sealed inside the pan along with the polymer coating [24]. The silica fiber does not suffer any state transition in the range of temperatures studied. The performed measurements had a span of temperatures ranging from 40 ºC to around 300 ºC.

When a sample of PVDF is melted for the first time, the crystal phase disappears, and when cooled, it may settle in a different phase form the starting one. If there is the need to repeat the DSC analysis in some of the samples, a new pan with a new sample of polymer is required.

The different phases of PVDF present different melting temperatures, some of the reported melting temperatures are shown in the Table 3-II. Notice that the melting temperature values for the α-phase and for the β-phase are essentially the same, around 170 ºC. Comparing the shape and width of the state transitions, the β-phase to melt transition is wider than the α-phase to melt transition [21,25].

PVDF Phase	DSC Melting Temperature T_m (ºC)
α	167-172
β	167-172 (broader)
γ	179-180

Table 3-II - DSC Melting Temperatures for important PVDF phases

3.3.1 Thin films

The DSC data was acquired in the heating process from 80 ºC to 300 ºC at a constant rate of 30 ºC/min. The chosen rate a high one, the phase transition is a dynamic process, this way the differential calorimetry curve may present and while a very wide transition may appear and difficult the determination of the DSC melting temperature value. Nonetheless, these measurements can lead to the observation of the temperature range where the transition takes place.

In the Figure 3.3 and Figure 3.4, the curves for 30 ºC/min rate are presented. The transition takes place from nearly 140 ºC to approximately 180 ºC for TF25_1 and from 130 ºC to 180ºC for TF25_2. The TF70_2 sample in the Figure 3.5 shows the same behavior as the sample TF25_1, 140-180 ºC.

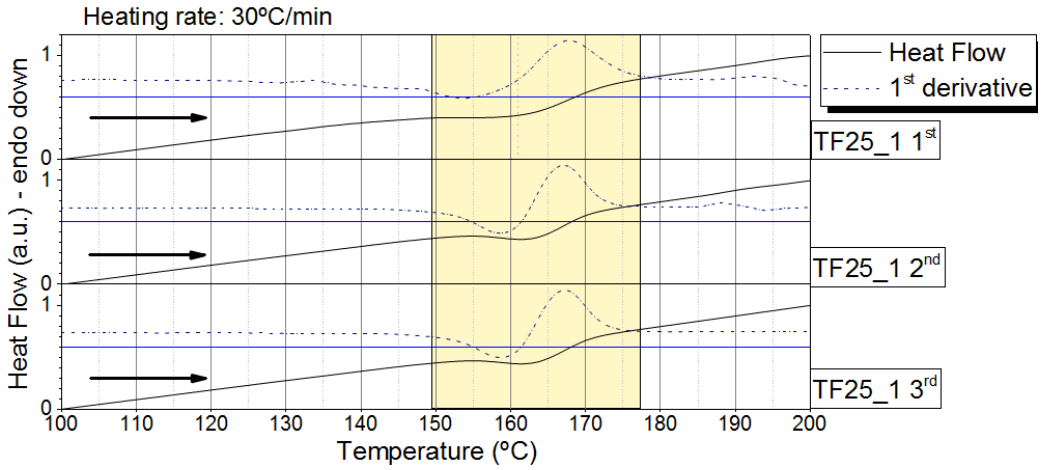

Figure 3.3 - 30 ºC/min rate DSC measurement for the TF25_1 thin film

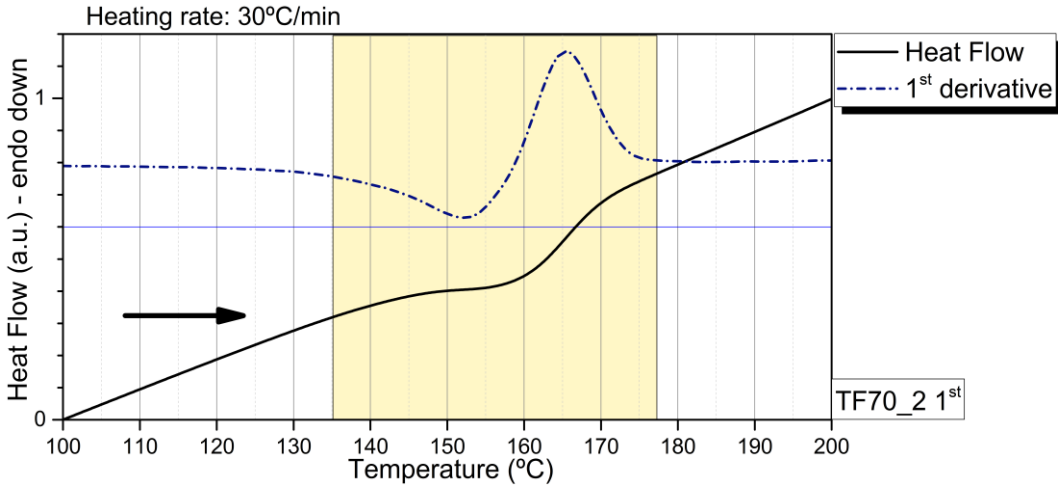

Figure 3.4 - 30 ºC/min rate DSC measurement for the TF25_2 thin film

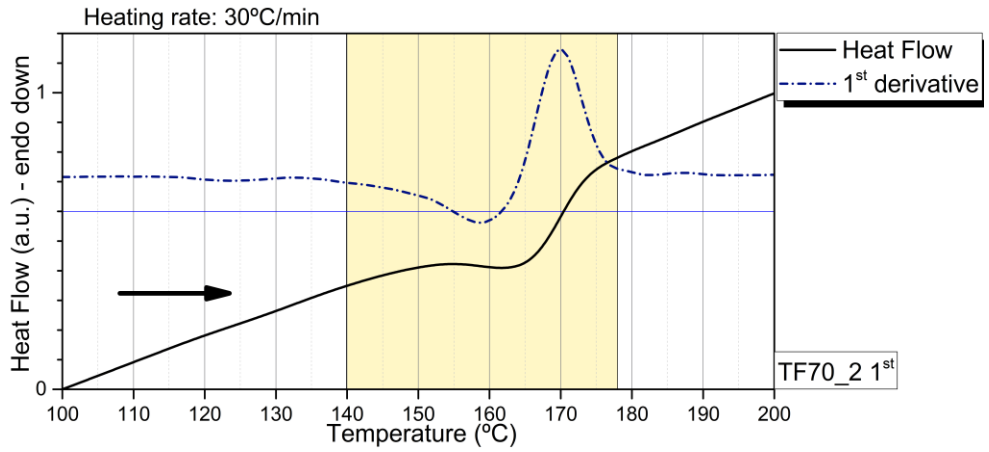

Figure 3.5 - 30 ºC/min rate DSC measurement for the TF70_2 thin film

The same samples were heated again, but this time the applied heat rate was of 1ºC/min, the acquired curves for the thin film samples are presented in the Figure 3.6. In the figure's plot the first derivative of each sample's curve has been included.

The derivatives seem to show a variation of the main curve slope at around 167 ºC for all samples, which is the span of the reported DSC melting temperatures for both the α-phase and the β-phase. Also, the variations tend to resemble an endothermic process, which is the expected kind of a melting phase transition, the results are presented in the Table 3-III.

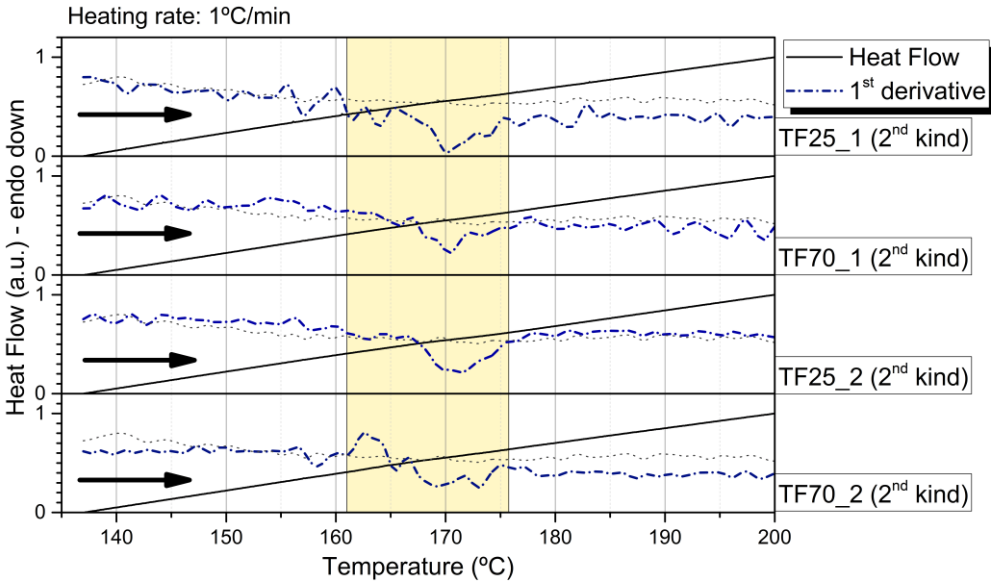

Figure 3.6 - 1 ºC/min rate DSC measurement for PVDF thin films

Sample	DSC 1st T_m (ºC)	Phase ID
TF25_1	167.9	α or β
TF25_2	167.6	α or β
TF70_1	167.9	α or β
TF70_2	167.1	α or β

Table 3-III - PVDF in thin films DSC melting temperature for 1 ºC/min constant heating rate

The samples TF25_2 and TF70_2 were subjected to further testing, a third heating curve at 5 ºC/min was plotted for each sample which can be seen in Figure 3.7. It is possible to observe the melting of the polymer in each of the plots as expected. The span of temperatures where the transition takes place is roughly the same as for the ones of the curves relative to the first heating process. Notice that the shape of both curves changes relative to the ones of the first heating, this may be an indicator of a change in the PVDF phase between the beginning of the first and second tests [26–28].

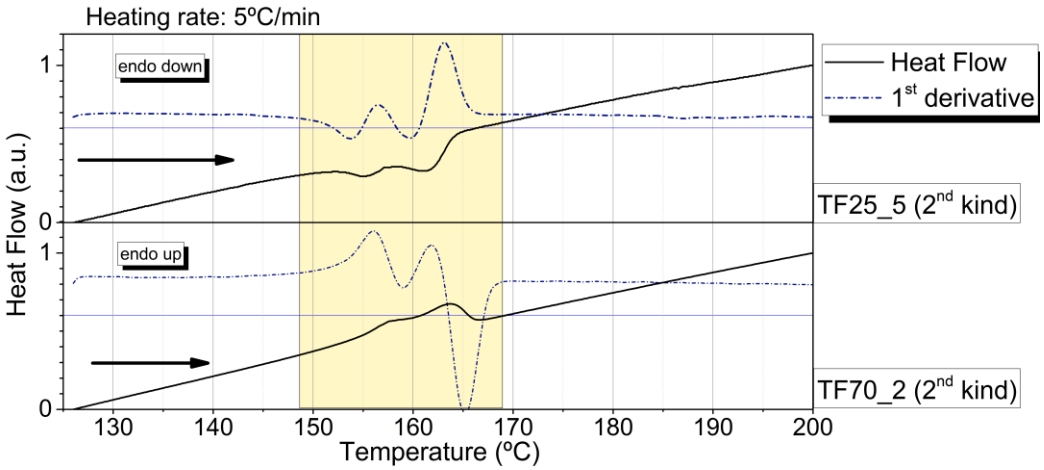

Figure 3.7 - Second DSC measurement for the thin films at 5 ºC/min rate

Another complete set of DSC samples from the same group of samples was heated again at a constant rate of 10 ºC/min. The results of the first heating cycle are presented in the Figure 3.8. The first derivatives have been plotted because they allow a simpler identification of transitions against the experimental curves. The baseline curve has been included to detect possible contaminations and help identify the transitions in the thin films exclusively.

There is a phase transition detected in the range 160-177 ºC. The melting of the PVDF takes place in the same range of temperatures as the first heating curve acquired at 30ºC/min. The DSC melting temperature can be identified as PVDF in the β-phase or in the α-phase.

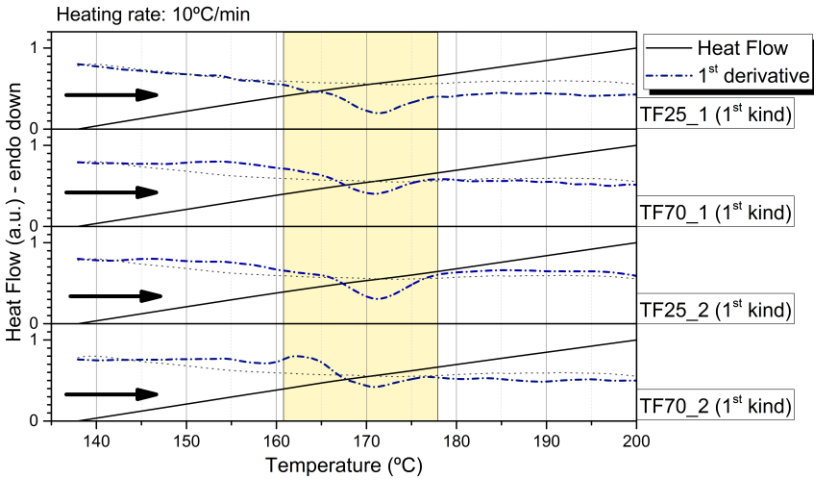

Figure 3.8 - 10 ºC/min rate DSC measurement for PVDF thin films

3.3.2 Optical Fibers

The quantity of PVDF in each pan for the Optical Fiber samples is very reduced compared with the quantity used for the thin films. The samples were measured in heating cycles ranging from 100ºC to 200ºC with rates of 5 ºC/min and 10 ºC/min. The experimental measurements can be observed in Figure 3.9 for the first rate, and Figures 3.10 and Figure 3.11. In the Figures Figure 3.9 and 3.10, a second heating curve is also plotted[1].

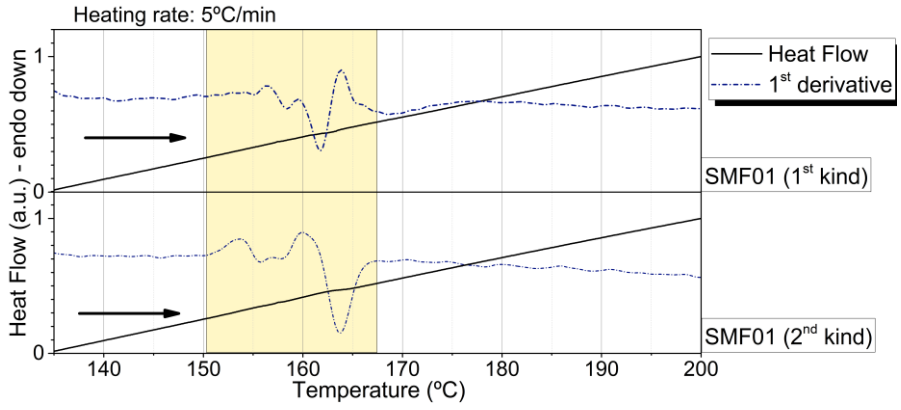

Figure 3.9 – DSC 5ºC/min measurements for SMF1

[1] During this measurement the sample pan and the reference pan were switched, thus an endothermic phase transition has the opposite concavity from other measurements.

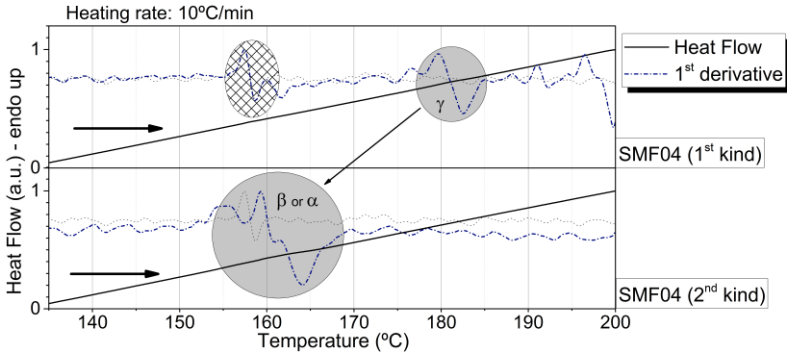

Figure 3.10 - DSC 10ºC/min measurement for SMF4

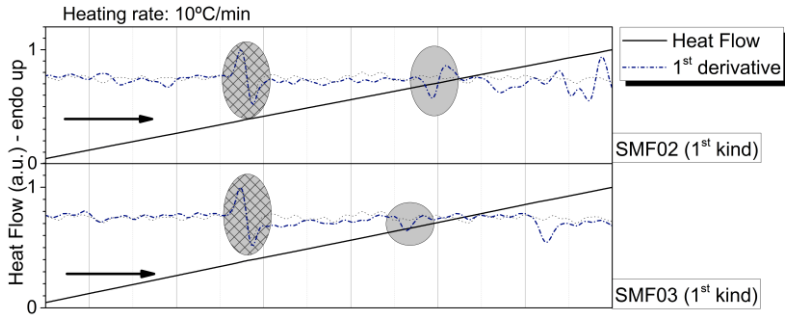

Figure 3.11 - DSC 10ºC/min measurement for SMF2 and SMF3

The observed DSC temperature due to phase transitions are presented in the Table 3-IV. The possible transition located near 159ºC has not been considered due to its presence in the reference curve, also plotted in the Figure 3.10. The transition may be due to some impurity in the DSC apparatus which is present during all the measurements in the Figure 3.10. The identification of the PVDF phases is also difficult because the transitions are not very pronounced and they may be masked or confused with other variations in the measurements caused by other sources.

Sample	DSC T_m (ºC)	Phase ID
SMF1	162.5	α or β
SMF1 (2nd)	162.5	α or β
SMF2	180	γ
SMF3	178	γ
SMF4	180	γ
SMF4 (2nd)	164	α or β

Table 3-IV - PVDF in Optical Fibers DSC melting temperature

3.4 X-Ray Diffraction (XRD)

The characteristic XRD spectra for the PVDF and respective peaks for different phases have been already identified. For the most interesting phases, as reported in literature, the information regarding the wavelength of characteristic peaks is present in the Table 3-V [29]. The detection of these phases may be done observing and linking the values of the peaks in the measured XRD data with the ones from the table.

3.4.1 Optical Fibers

In order to perform a XRD measurement in the optical fiber, two different types of samples were prepared: the first type consisted in the PVDF-free optical fibers, and the second type had the fibers coated with PVDF in the tip. Both types of samples had several optical fibers put together in the substrate, so that the sampling area is maximized. Both samples were measured in the same conditions in order to detect differences between the data of the two curves. If differences are detected, they may be justified by the presence of PVDF in the sample.

The experimental data from the XRD measurements of the both samples can be seen in Figure 3.12. The overall spectrum of each sample is approximately the same, with prominent peaks at diffraction angles of 2θ with values of 14.5º, 17.4º, and 26º.

Phase	2θ (º)	Crystal Plane
α	17.66	(100)
	18.30	(020)
	19.90	(110)
	26.56	(021)
β	20.26	(110) (200)
γ	18.50	(020)
	19.20	(002)
	20.04	(110)

Table 3-V - X-ray diffraction angles for different PVDF phases and correspondent crystal planes

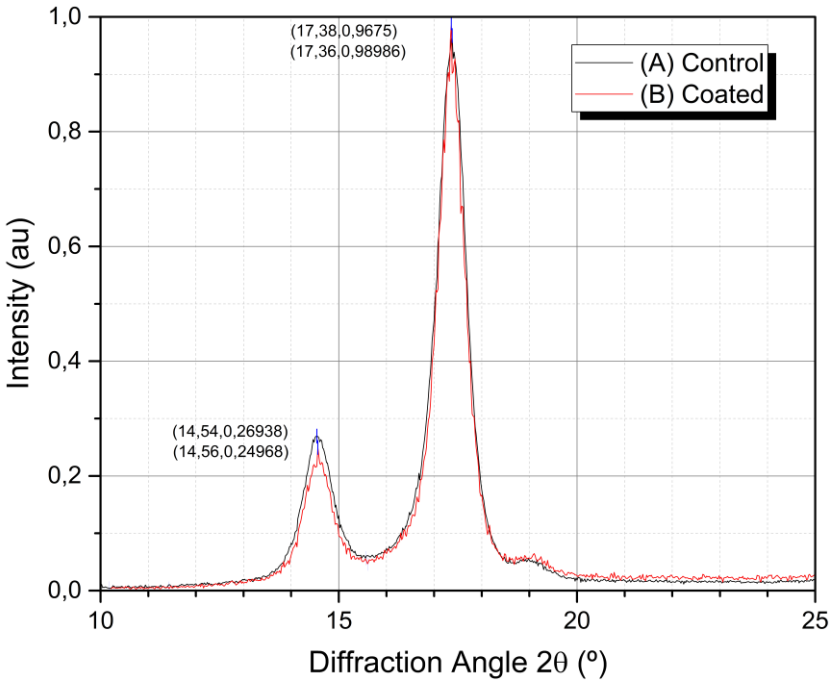

Figure 3.12 - XRD data for the Optical Fiber samples

Considering the fact that both the quantity of polymer deposited in the tip of the fibers is very small, and the area where the polymer is deposited is very small compared to the non-deposited fiber, the spectrum is essentially the same as the one of non-coated fibers. The coated sample is presented in the Figure 3.13, in a good case scenario, taking only in account only the exposed fiber and the coated fiber, for a 3-centimeter-long exposed fiber and the length of the coated fiber roughly 5 millimeters long, the fraction of the PVDF coating is approximately 17%.

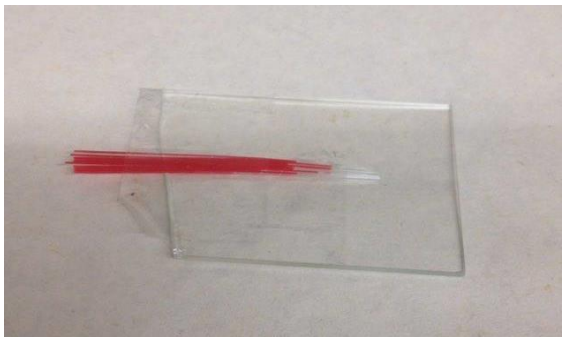

Figure 3.13 - Optical Fiber XRD sample

3.4.2 Thin Films

In the case of the thin films, two samples were also submitted to a XRD measurement. Both samples were coated with the same PVDF solution. The difference between the two samples is in the drying temperature, after the coating process, which was differed for both samples. The respective temperatures for the drying process were 25ºC for the first type, and 70ºC for the second type.

In the Figure 3.14 one can see the two curves for the measurements performed in both samples.

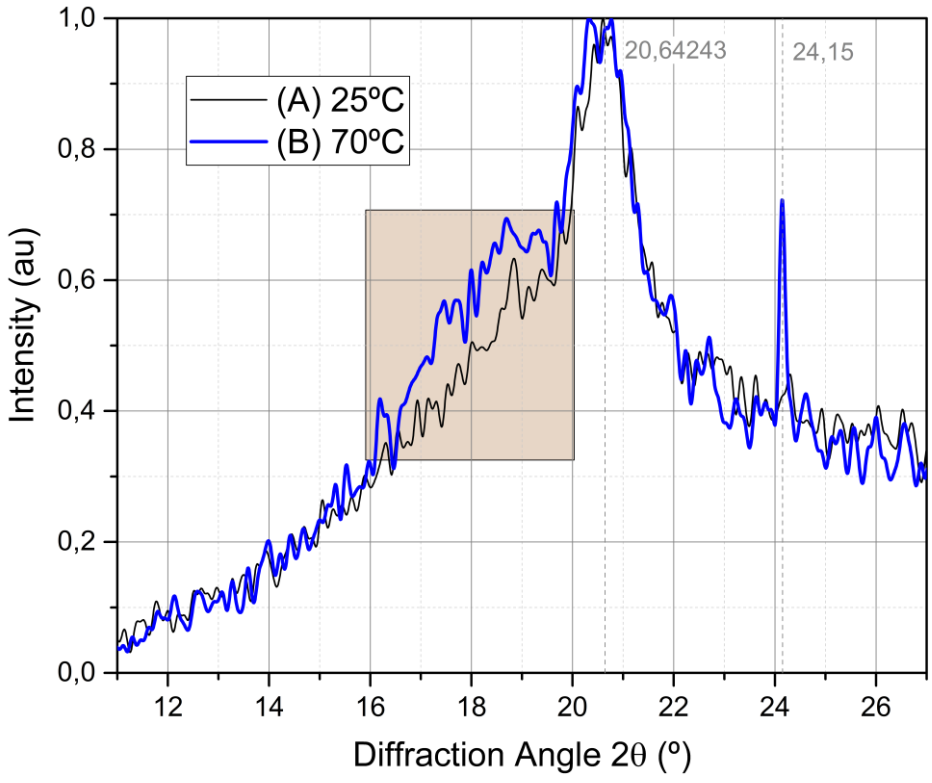

Figure 3.14 - Thin Film samples' XRD diffractogram for different drying temperature

Both measurements seem alike, there is a common peak at 20.5º. A peak centered at 24.0º is also present for the substrate that was annealed at 70ºC, this peak was not considered for the qualitative analysis due to its FWHM discrepancy from the prior. A mild shoulder located near 18.5º is observable. This shoulder is related both to an amorphous phase, or the α and the γ phases of PVDF [30,31].

Another main difference between the two can be immediately observed by visual analysis where the second sample, the annealed one, is almost transparent for visible wavelengths, whereas the first sample is white-opaque.

3.5 Fourier Transform Infrared Spectroscopy (FTIR)

Another technique used to analyze the PVDF samples was the Fourier Transform Infrared Spectroscopy (FTIR) where an Infrared (IR) beam with the help of a prism are used to probe the sample for absorption at long wavelength. The FTIR technique used is based on the effect of Attenuated Total Reflectance (ATR), which lets the sample be probed by simply clamping it to a crystal, part of the machine, where the IR beam will propagate. This lets the measurements to take place without need to pre-prepare the sample in a specific way.

The different samples of PVDF present different absorption bands with different amplitudes depending on the existent phases and each phase's quantity. The characteristic peaks for the principal phases are presented in the Table 3-VI. With the help of this values the sample can be qualitatively characterized.

PVDF Phase	Absorption Bands wavenumber (cm^{-1})
α	408, 532, 514, 766, 855, 976
β	449, 463, 510, 840, 930, 1279, 1347
γ	431, 512, 776, 812, 833, 840, 1234

Table 3-VI - Characteristic Wavenumbers for different PVDF phases in FTIR analysis

3.5.1 Thin Films

Different samples of first type, PVDF deposited over substrates, were measured. The data acquired during the process is plotted in the Figure 3.15. To help identify the phases that may compose the samples, vertical guidelines have been added to the plot with the values of the Table 3-VI. All the samples show absorption bands at 1234 (cm^{-1}) relative to the γ-phase. There is also a shoulder present for some of the samples from an absorption band at 1279 (cm^{-1}) relative to the β-phase.

The experimental data does not present any absorption at the values relative to the α-phase absorption bands.

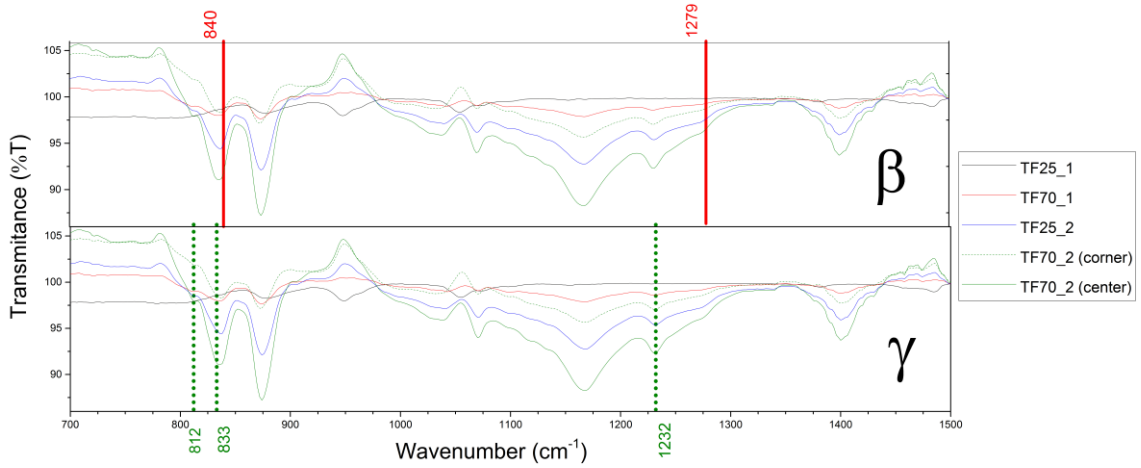

Figure 3.15 – Thin Film samples' FTIR spectra 700-1500 cm^{-1}

In order to better analyze the data near in the 790-900 (cm^{-1}), a separate plot regarding these wavenumbers is plotted in Figure 3.16. In this part of the spectrum the two absorption bands at 812 (cm^{-1}), 833 (cm^{-1}) for the γ-phase, and 840 (cm^{-1}), for the β-phase, may be observed.

Once again, for all samples, the absorption at the γ-phase values is more prominent. There may be some contribution at 840 (cm^{-1}), but it may be only because a broadening near the 833-840 (cm^{-1}) range [32,33]. The 855 (cm^{-1}) band does not seem to be present as expected after observing the Figure 3.15.

The four PVDF thin films deposited in the substrates using the same methodology seem to have a predominant presence of PVDF in the γ-phase, the β-phase seems to be also present, but in lower quantity.

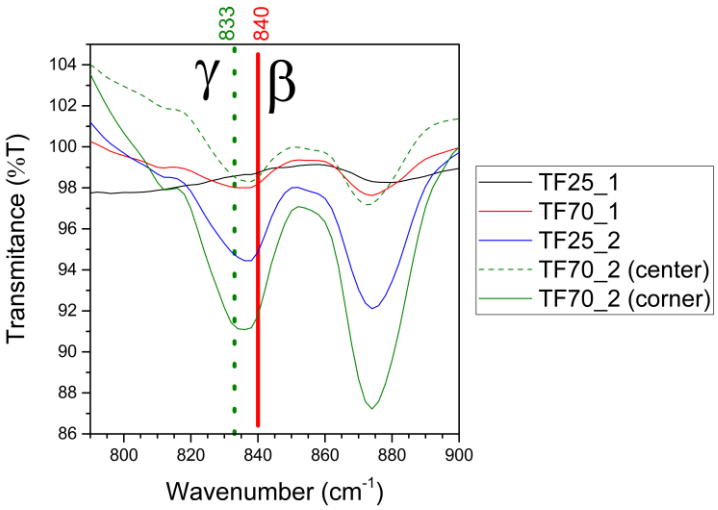

Figure 3.16 - Thin Film's FTIR data detail at 790-900 cm^{-1}

3.5.2 Optical Fibers

In the case of the optical fibers, four samples produced with the dip coating methodology described were tested in the FTIR-ATR. In Figure 3.17 the experimental measurements of the FTIR-ATR technique are plotted. Similarly, the same set of vertical lines correspondent to the most important phases of PVDF were added to help characterize the samples, has it was done for plots of the thin films. The curves do not show to have absorption at the α-phase values. The two bands at 1234 (cm^{-1}) and 1279 (cm^{-1}) are visible for all samples, this suggests the presence of both γ-phase and β-phase in the samples.

Focusing now on the narrower spectrum band plotted in Figure 3.18, the absorption band at 840 (cm^{-1}) from the β-phase seems to be stronger than the one from the γ-phase at 833 (cm^{-1}) that is reported to cause the broadening the overall curve.

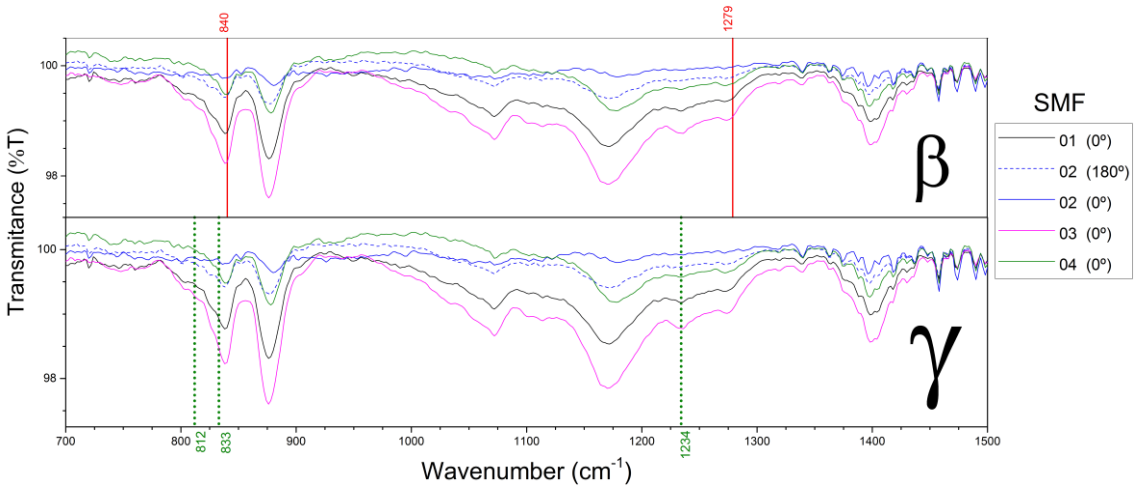

Figure 3.17 – Optical Fiber samples' FTIR spectra 700-1500 cm^{-1}

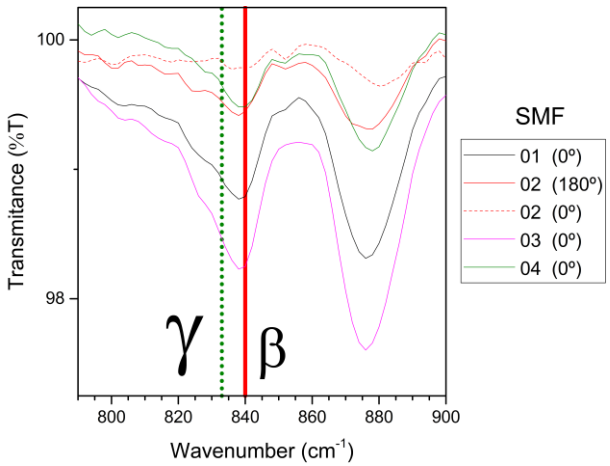

Figure 3.18 – Optical Fiber's FTIR data detail at 790-900 cm^{-1}

3.6 Concluding Remarks

In order to have an overview in the results of the three characterization methods, the results are synthetized in the Table 3-VII for the thin films and in the Table 3-VIII for the coated SMF.

The method that provided a simpler measurement process and analysis was the FTIR technique. This technique allowed the identification of PVDF phases for both thin films and optical fibers. Even with very little quantity of PVDF deposited, mainly in the SMF, the FTIR-ATR was able to acquire satisfactory data compared with the data acquired with the thin films.

In the case of the DSC, the method was able to detect the melting of the polymer but the curves had very different shapes depending on the rate used to heat the sample. The experimental data needed a more careful analysis that did not always provide an exact conclusion. These difficulties are mostly verified for the coated SMF, where the quantity of polymer used tin the measurements is very little. In the case of the thin films the main factor that contributed to some doubts was the heating rate used. The rate that exhibit the best results was the 10 ºC/min.

The XRD technique was not able to analyze the coated SMF, possibly due to the small quantity of PVDF compared to the SMF itself. There was no difference between the control spectrum and the sample's spectrum. The technique did not allow a positive identification of either phases of PVDF. The thin film's analysis was more similar to the one presented in the literature. The expected peaks did not appear as strong in the measurements as expected, the phase identification was made through a comparison of the XRD experimental curve's shape and the shape of other curves in the literature. The spectra of the thin films suggest a mixture of phases.

Sample	DSC	XRD	FTIR	Final ID
TF25_1	α or β	β or γ	β but mostly γ	γ and some β
TF25_2	α or β	β or γ	β but mostly γ	γ and some β
TF70_1	α or β	β or γ	β but mostly γ	γ and some β
TF70_2	α or β	β or γ	β but mostly γ	γ and some β

Table 3-VII - Phase identification in thin films

Sample	DSC	XRD	FTIR	Final ID
SMF1	α or β	---	β and γ	β and some γ
SMF1 (2nd)	α or β	---		
SMF2	γ	---	β and γ	β and some γ
SMF3	γ	---	β and γ	β and some γ
SMF4	γ	---	β and γ	β and some γ
SMF4 (2nd)	α or β	---	β and γ	

Table 3-VIII - Phase identification in coated SMF

Overall, from the three methods, the one that provided a more certain analysis was the FTIR-ATR technique. The XRD and the DSC address some hints related with the FTIR-ATR analysis.

Nevertheless, it was possible to identify the presence of PVDF in both γ-phase and β-phase. As expected, the solvent casting from PVDF/DMF produces essentially these two phases, that are important to the scope of the present work. The relative quantity of the most electroactive phase, the β-phase, is also higher for the coated SMF, possibly due to the cylindrical geometry of the fibers.

4 Optical Characterization of a PVDF Fabry-Perot

4.1 Introduction

In this chapter, the production of an optical sensing device based in PVDF technology is explored. Throughout the chapter the main steps taken in order to achieve the objective are presented.

In a first approach, the PVDF is used to coat a cleaved end of the optical fiber as suggested in the Figure 4.1, which is a similar design to the Parylene-C polymer Fabry-Perot proposed in the literature [34]. Compared to the sensor proposed in the literature, that has high reflectivity gold mirrors in the interfaces, the polymer will form a small intrinsic low finesse Fabry-Perot cavity.

Figure 4.1 - Intrinsic Fabry-Perot cavity configuration

A low finesse Fabry-Perot principle lies in the interference pattern that arises from the optical path difference between the reflection in the first interface (SMF/PVDF) and the second interface (PVDF/air). The reflection coefficients depend only in the index of refraction difference at each interface and can be calculated by the Fresnel equations, considering perpendicular incidence to the interfaces. The reflected wave can be described as indicated in the following equation [10].

$$I_r(\lambda) = I_1(\lambda) + I_2(\lambda) + \sqrt{I_1(\lambda)\, I_2(\lambda)} \cos[\, \phi(\lambda, t_{\mathrm{PVDF}}) \,], \tag{4.1}$$

where I_1 and I_2 stand for the intensity of beam 1, from the first interface, and beam 2, from the second interface. The phase difference between the two waves due to optical path difference in the PVDF is represented by ϕ and depends on the thickness, t_{PVDF}, of the polymer.

The free spectral range of the spectrum's peaks, $\Delta\lambda$, will directly depend on the thickness of the PVDF. After some mathematical manipulation, considering the operating wavelength, $\lambda_{\mathrm{operation}}$, the relation between these parameters is given by:

$$t_{\mathrm{PVDF}} = \frac{\lambda^2_{\mathrm{operation}}}{2n \cdot \Delta\lambda} \tag{4.2}$$

4.2 Intrinsic Fabry-Perot cavity fabricated by dip coating

The device was produced trough a dip coating technique. The SMF was first cleaved and then dipped in a PVDF/DMF solution, in order to deposit a thin film of the PVDF polymer in the top part of the fiber. The result of this dip coating is a short Fabry-Perot cavity that produces a long period response. The reflected optical power spectrum is shown in the Figure 4.2. The length of the FP, t_{PVDF}, has been estimated by performing a Fabry-Perot fit given by equation (4.1) in order to extract the period. Then, using the equation (4.2), the length of the PVDF's thin film has been calculated considering the PVDF index of refraction ($n_{\mathrm{PVDF}} = 1.41$).

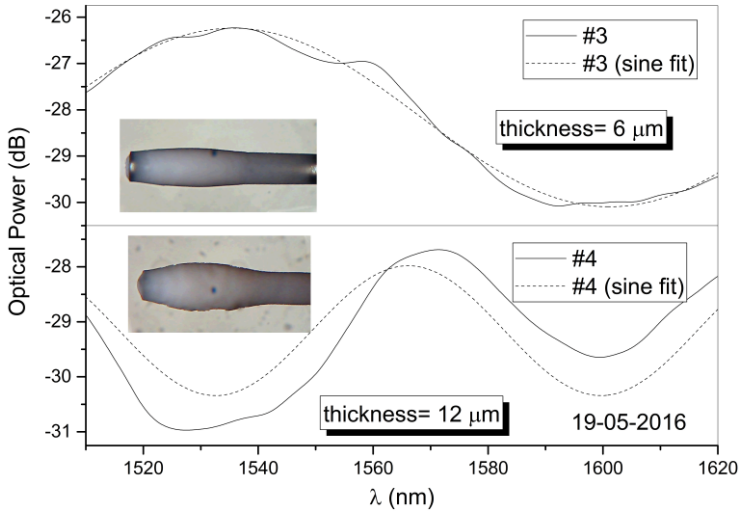

Figure 4.2 - Intrinsic PVDF Fabry-Perot Cavity Spectrum

A white light source was used to illuminate the SMF in order to be able to observe the fiber's core before and after the coating process (see Figure 4.3). The initial cleaved SMF, in the left, restricts the light propagation to the fiber's core. With a thin film deposited in the top of the fiber, the dispersion of the light in the PVDF is visible.

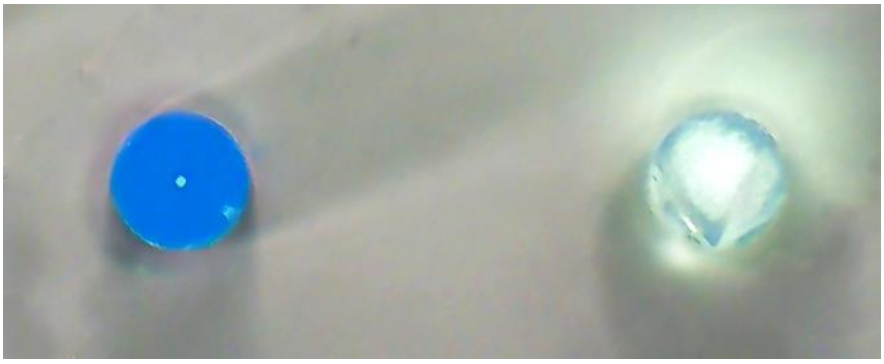

Figure 4.3 - Top view of cleaved SMF (left) and coated SMF (right)

4.3 Fabry-Perot Cavity in the tip of the optical fiber

Adding a hollow tube spliced to the SMF's tip and then depositing PVDF in the open end of the tube, a FP is formed. The FP's mirrors are the two interfaces: between the SMF and the tube; and between the tube and the thin film of polymer.

The device is formed by the FP cavity between a cleaved end of a SMF and a thin film of PVDF. In Figure 4.4, a schematic of the device is presented, where the SMF is represented by the dark grey part, whereas the hollow tube is the transparent section and in red is represented the thin polymer film deposited in the top part of the device.

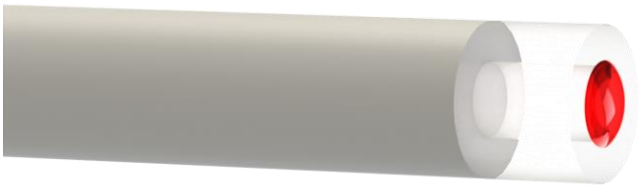

Figure 4.4 - Fabry-Perot cavity design in the tip of the SMF

In order to create the design proposed in Figure 4.4 a standard SMF was cleaved and spliced with a portion of hollow silica tube. The tube was also cleaved, producing a hollow-fiber tip. The dip coating in the PVDF/DMF process can be seen in the Figure 4.5.

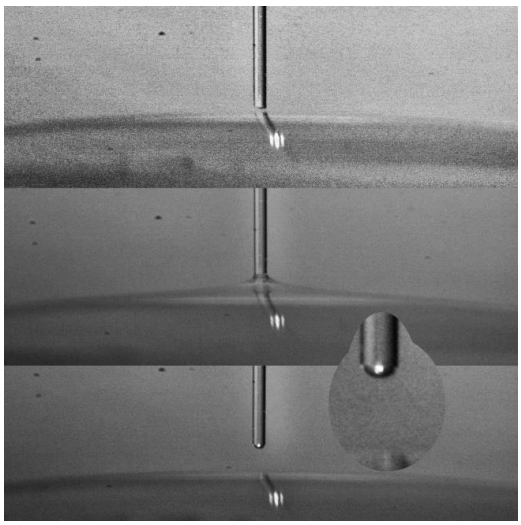

Figure 4.5 - Precision dip coating of the SMF tip

The hollow-fiber tip was placed in a perpendicular orientation to the horizontal plane using a microscope setup with a vertical precision adjustment screw, depicted in the Figure 4.6. First, the fiber was carefully lowered, until the tip slightly plunged a drop of PVDF/DMF solution placed over a microscope slide. (The solution rapidly involves the lateral wall due to the capillarity effect). The tip was shortly risen and the crystallization process begins, forming the Fabry-Perot cavity.

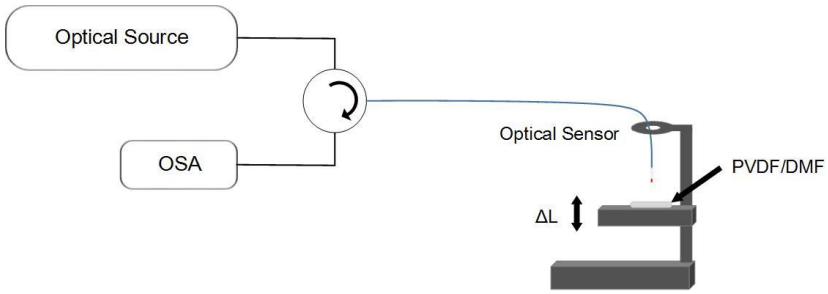

Figure 4.6 – Setup for Fabry-Perot fabrication monitoring

The setup in Figure 4.6 was used to monitor the evolution of the cavity during the process. The setup configuration is constituted by a broadband source centered at 1550nm with a bandwidth of 100nm used to light the setup. One optical circulator is used to read the reflected signal of the Fabry-Perot. The OSA measures and plots the FP's spectrum. The evolution of the response spectrum of the cavity can be observed in the Figure 4.7, where a FP-like spectrum is visible after the quick drying process of the deposited PVDF thin film. A comparison with the non-coated fiber is also present in the figure.

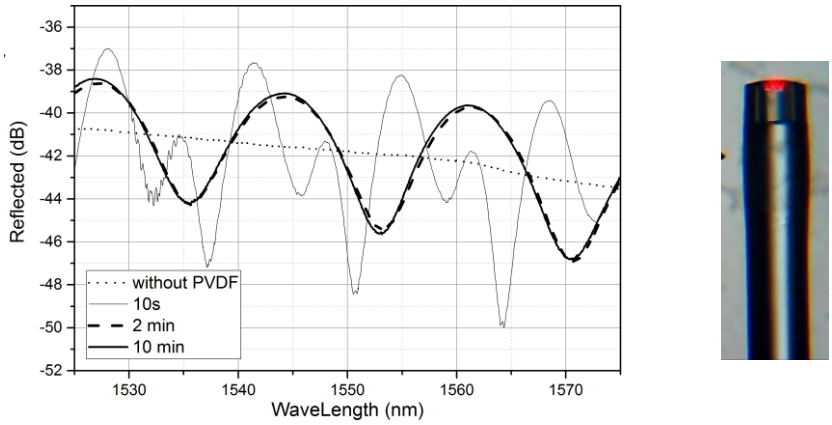

Figure 4.7 - Spectrum evolution during drying the process (FP#1)

The cavity was observed before and after the polymer's deposition. In the Figure 4.8 on the left, the hollow portion of the fiber that was previously fusion spliced with the SMF has an open end. After the deposition process the cavity was observed again in the same microscope. This time, in order to have more contrast between the tube and the polymer, a visible He-Ne Laser centered at 633 nm was used to light the other end of the SMF so that the beam is dispersed in the PVDF. The final FP, with thin film of PVDF, can be seen in the right part of the Figure 4.8.

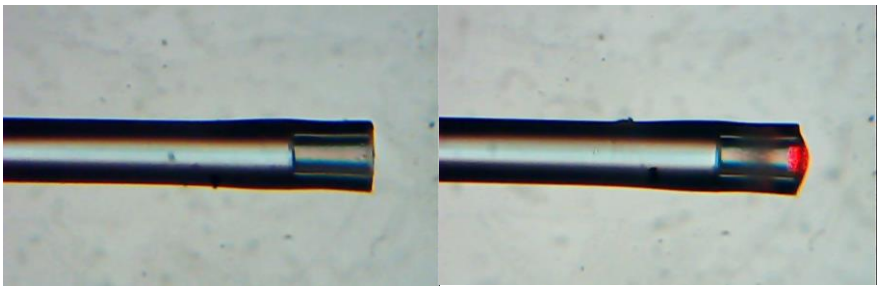

Figure 4.8 - Hollow tube (left) and FP cavity (right) under the microscope (FP#3)

Several devices were produced so that the repeatability of the process was confirmed. However, the different devices have different lengths of the hollow portion of the cavity, therefore varying the length of the cavity itself. The length of the produced cavities and the thin film thickness were measured under de microscope. In the Appendix C, a 3-wave interferometer model for the cavities was used to estimate these parameters, considering both the air propagation and the PVDF's thickness [35]. Performing a fit to the reflected spectrum of each cavity it is possible to reproduce the spectra of various samples and confirm the measurements. The values for both measurements are condensed in the Table 4-I.

Cavity	**Tube length (μm)**	**Cavity length (μm)**		**TF thickness (μm)**	
	Microscope	Microscope	Estimated	Microscope	Estimated
01	84	65	65	23	23
02	203	200	200	~0	~5
03	158	137	140	18	18
04	71	61	60	20	20

Table 4-I - Cavity length and Thin Film Thickness

Some of the fitted spectra can be seen with their experimental counterpart in the Figure 4.9 and Figure 4.10.

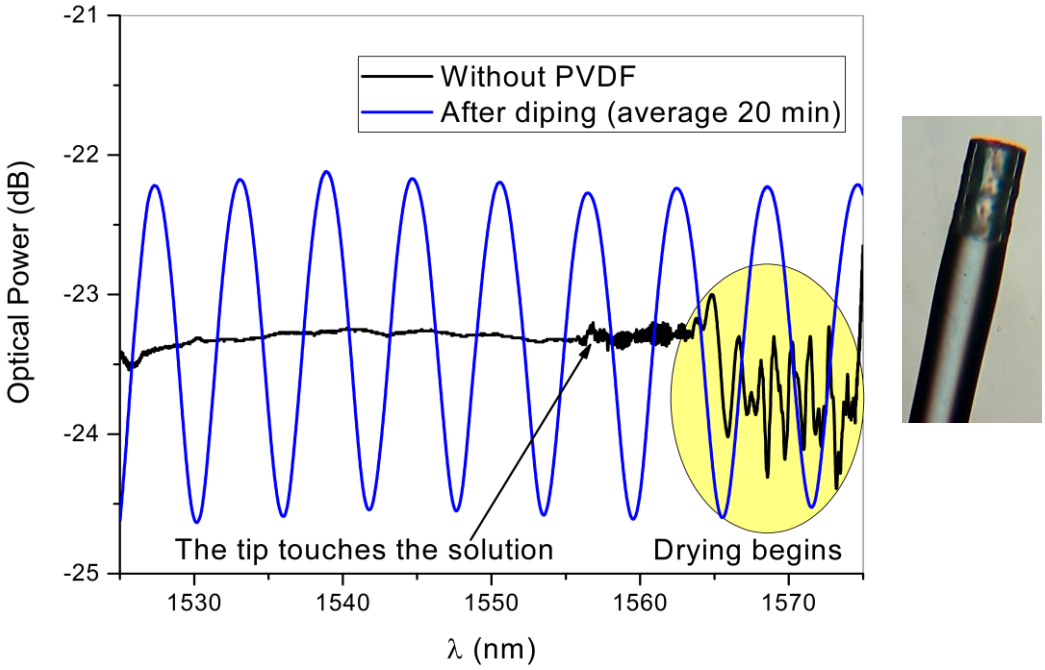

Figure 4.9 - Real-Time spectrum of the cavity FP#2

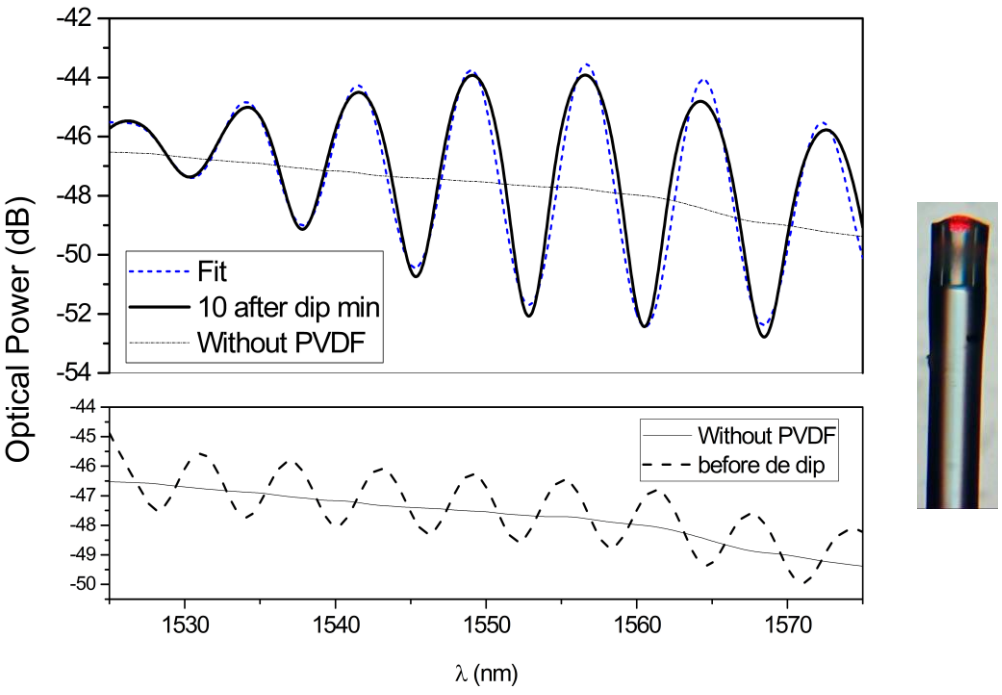

Figure 4.10 - Real-Time spectrum of the cavity FP#3

4.4 Temperature Tests

The cavity labeled as FP#2 was tested in the lab for its temperature response using the experimental setup represented in the Figure 4.11. Although humidity is not a controlled parameter in the lab and may interfere in the measurements, the experiment was done. The shift of the maximum at 1550nm was monitored and analyzed. The multiple spectra acquired during the experiments are presented in the Figure 4.12. During the cooling process, there is an observable shift of the whole spectrum (to the right) from the shorter wavelengths to longer ones.

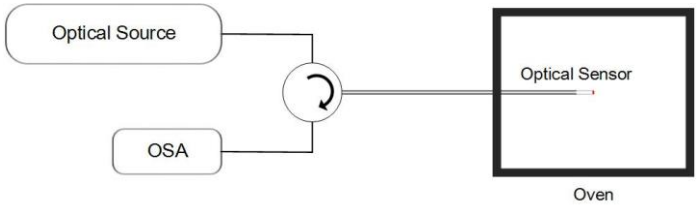

Figure 4.11 – Setup for Temperatue characterization

The evolution of the relative maximum's position from the Figure 4.12 is presented in the Figure 4.13. The behavior tends to be nearly linear for temperatures ranging between 50ºC and 30ºC. A linear fit was performed in this temperature range being the respective sensitivity of $-128\ \mathrm{pm/K}$ where the negative sign represents the direction of the shift[2], decreasing the wavelength as the temperature goes up.

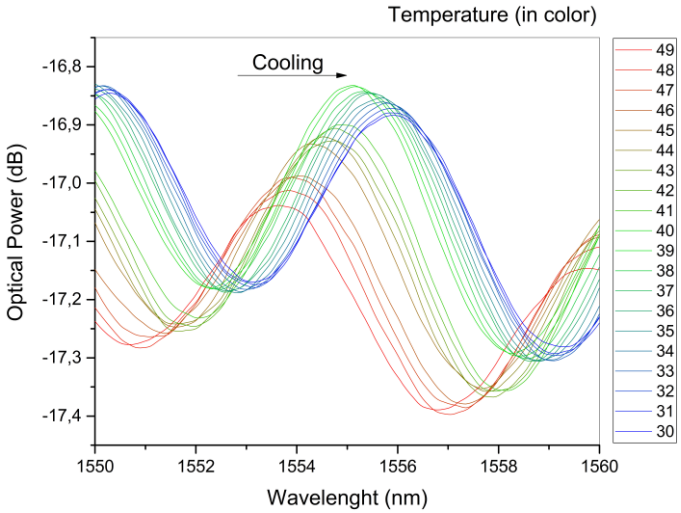

Figure 4.12 – Spectrum evolution for the oven temperature analysis (FP#2)

[2] The negative sign will be considered in the sensitivity value whenever a parameter (Temperature or Humidity) cause a shift to lower wavelengths.

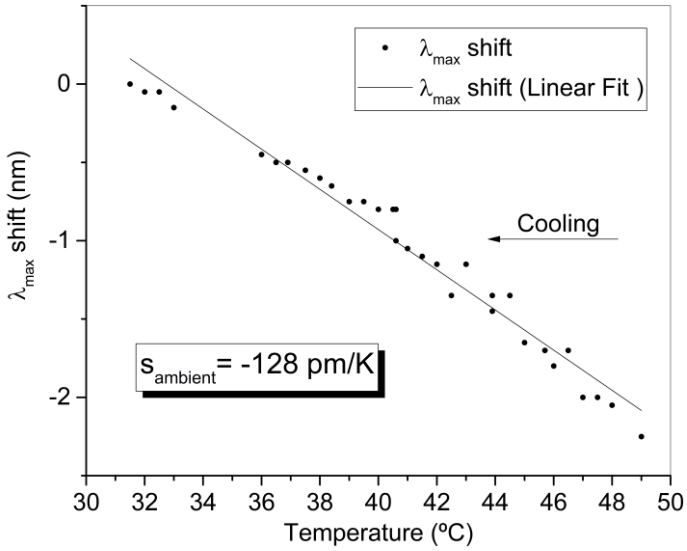

Figure 4.13 – Shift of the monitored maximum position during the cooling process (FP#2)

In order to have a full control of both parameters, the devices were subjected to simultaneous temperature and humidity tests using a *Fitoclima 300* Climatic Chamber in the experimental setup depicted in the Figure 4.14. Only two of the devices were taken to analysis due to heavy restrictions in the availability of the chamber and in the experimental setup, that can only read one sensor at a given time. The experimental setup is similar to the prior, but the oven has been substituted for the climatic chamber. A local PC controlled the OSA's measurement, and later retrieved the experimental data directly via GP-IB. In the Appendix B the program developed by me using the OSA datasheet is explained. The computer had an internet connection and provided a real-time monitoring in the restricted area were the experiences were running.

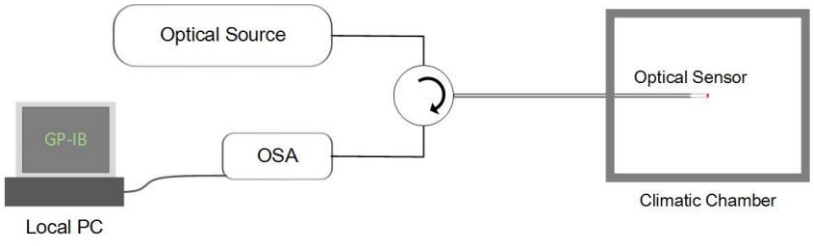

Figure 4.14 – Setup for Temperatue and Humidity characterization (with remote monitoring)

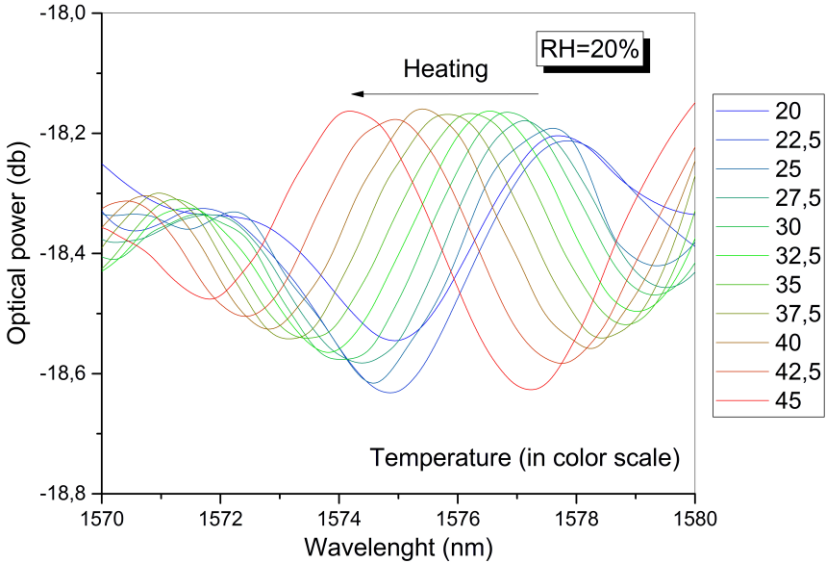

Figure 4.15 - Spectrum evolution for temperature variation (FP#2)

In the Figure 4.15, the evolution of the FP#2 spectrum for thermal variations is presented. The temperature was varied from 20 ºC to 50 ºC at a controlled relative humidity of 20 %RH. There's a visible shift from the longer wavelengths to the shorter ones (right to left) as the temperature rises. In this analysis, various peaks were monitored, as depicted in the Figure 4.16. The calculated average sensitivity has a value of -137 pm/K. As expected, the FP presented the same sensitivity as the temperature characterization run in the lab.

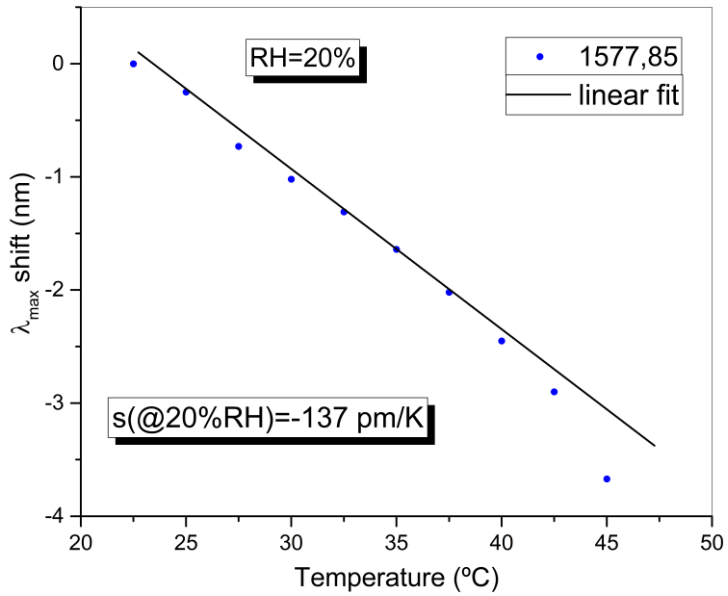

Figure 4.16 - Shift of the monitored maxima position during the heating process (FP#2)

Using the same sensor, a temperature variation from 40ºC to 60ºC was performed at a constant relative humidity of 70%. In the Figure 4.17, the inset graph presents the evolution of the spectrum during the experiment for the monitored peak. In the same figure the shift of the peak is shown, this time the sensitivity is reduced to -40 pm/K.

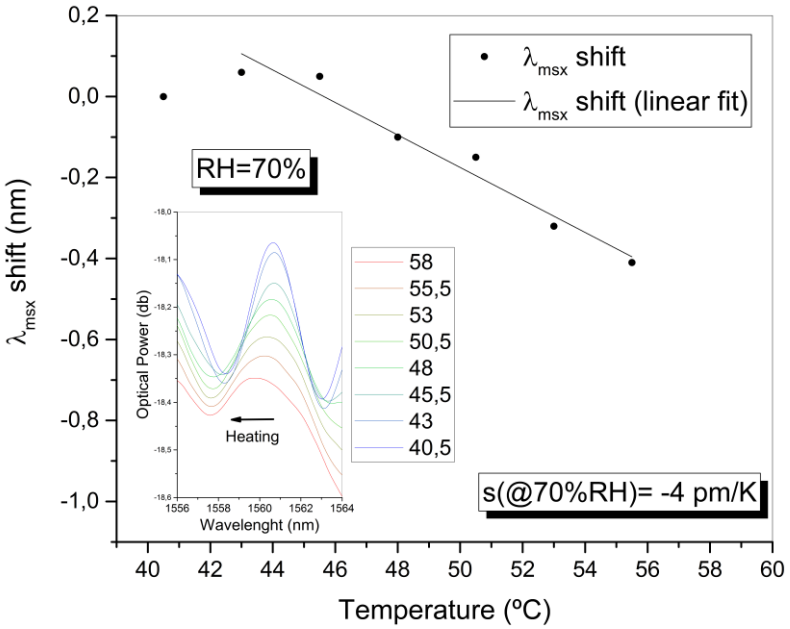

Figure 4.17 - Temperature characterization at 70%RH (FP#2)

The second sensor, FP#2 was also tested for temperature variation in a shorter temperature span, form 20ºC to 40ºC. Prior to this test, the relative humidity was risen to 80%. In the Figure 4.18, the evolution of the peak near 1562nm is presented, showing a positive sensitivity, from left to right as the climatic chamber is heated. The sensor has a sensitivity of $+27$ pm/K at a relative humidity of 80%.

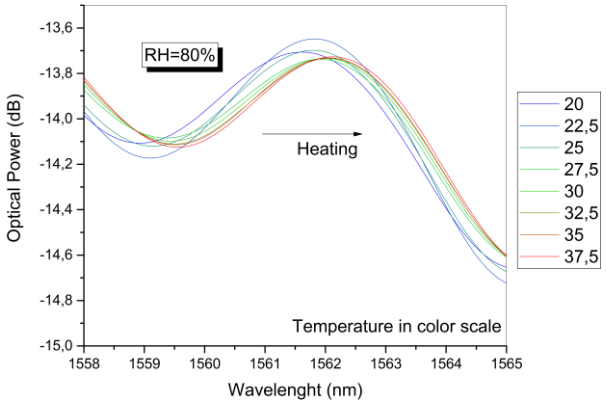

Figure 4.18 – Spectrum evolution for temperature characterization at 80%RH (FP#2)

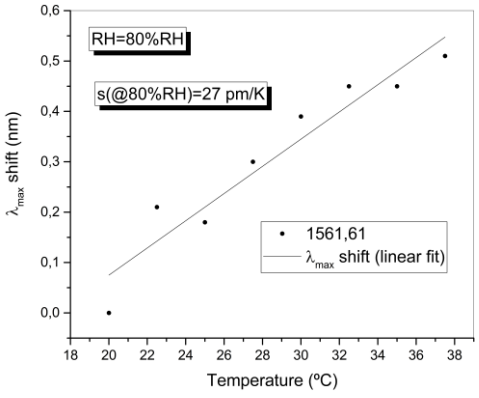

Figure 4.19 - Monitored peak's shift for temperature characterization at 80%RH (FP#2)

4.5 Humidity tests

The same Fabry-Perot cavity, FP#2, was subjected to a relative humidity variation a constant temperature of 20 ºC. The spectrum response, in the Figure 4.20, has a negative shift in the monitored peak at 1556 nm.

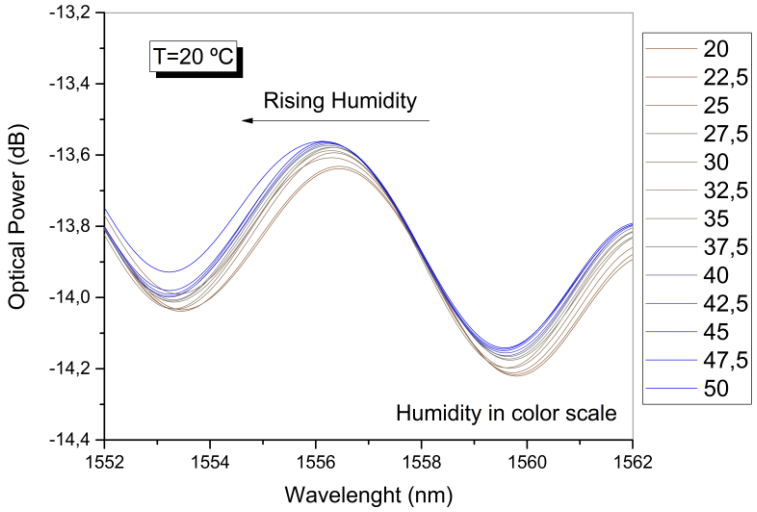

Figure 4.20 - Spectrum evolution for humidity variation at T=20ºC (FP#2)

The plot of the maximum shift is presented in the Figure 4.21. The calculated negative sensitivity has a value of $-9.3\ \mathrm{pm/\%RH}$

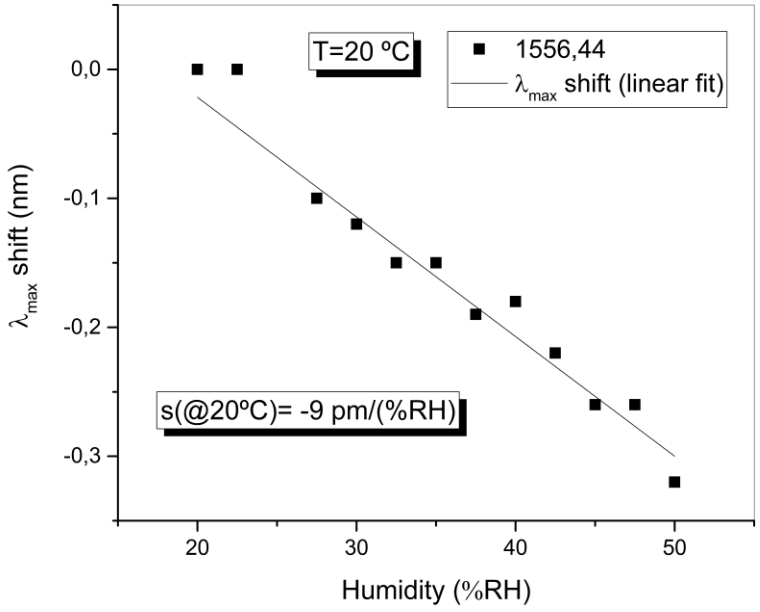

Figure 4.21 - Maximum shift for Humidity variation at T=20 (FP#2)

The FP#3 was also subjected to a relative humidity test at a constant temperature of 70 ºC with the humidity increasing from 30%RH to 80%RH. The spectrum shifts to the longer wavelength as the humidity goes up, as the plot in the Figure 4.22 shows.

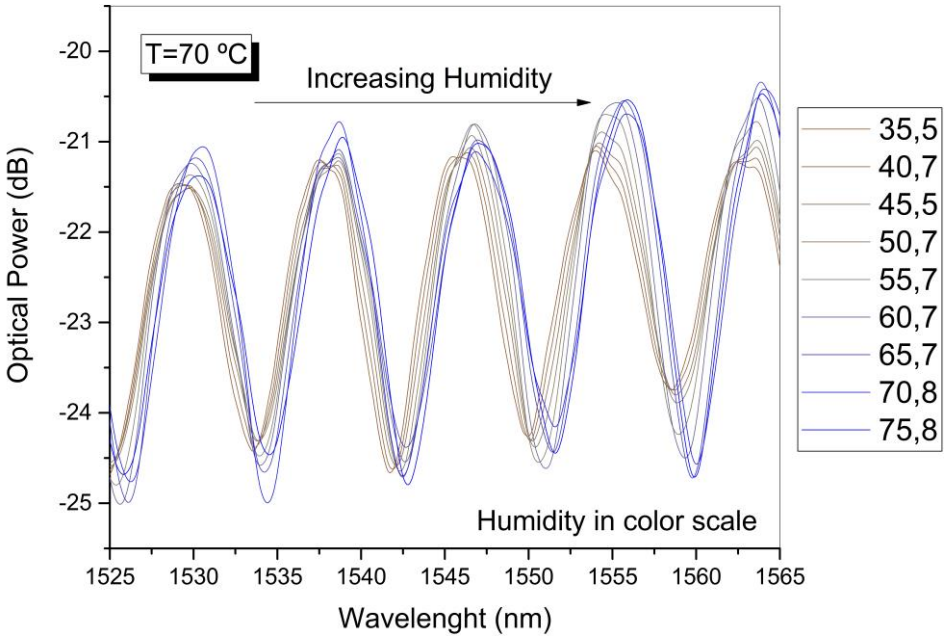

Figure 4.22 - Spectrum evotution during Relative Humidity variation at 70ºC (FP#3)

All the maxima were monitored, being the extracted sensitivity of $39.28\ \mathrm{pm/\%RH}$.

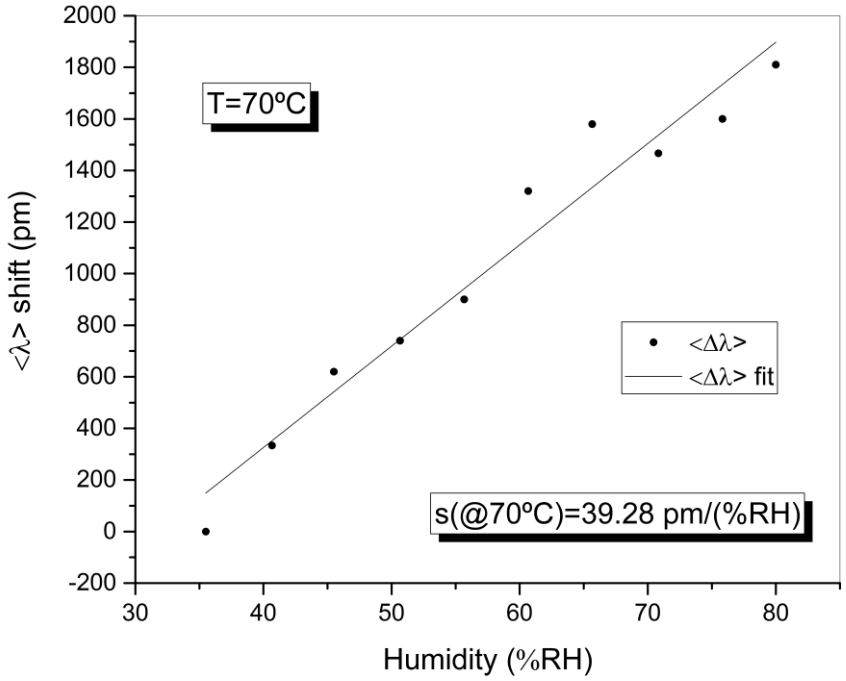

Figure 4.23 – Maxima's eaveleght shift caused by Relative Humidity variation at 70ºC (FP#3)

4.6 Concluding Remarks

It was possible to develop interferometric cavities using a precise dip coating technique. When the dip is not controlled, the fiber is submerged, and the PVDF tends to concentrate in the sidewalls of the SMF rather than in the end face of the fiber.

The intrinsic Fabry-Perots have a thickness inferior to 20 μm, thus having a greater free spectral range. Adding a hollow tube between the PVDF and the SMF's end face, allows a simple production of more complex cavities, that proved to be sensitive to Temperature and Humidity variations. The values of the sensitivities are condensed in two tables, in the Table 3-I the temperature characterizations, and in the Table 3-II, the relative humidity characterizations.

Constant Relative Humidity (%RH)	FP#2	FP#3
lab	-128 pm/K	---
20	-137 pm/K	---
70	-40 pm/K	---
80	27 pm/K	---

Table 4-II - Temperature sensitivities for the tested cavities

Constant Temperature (ºC)	FP#2	FP#3
20	-9.3 pm/%RH	---
70	---	39.28 pm/%RH

Table 4-III - Humidity sensitivities for the tested cavities

The variations in the sensitivity may be caused by the three-wave interference, that have a more complex analysis than those of two-wave interference. In order to better tune the parameters of the cavities for sensing applications, the sensors require more characterization under controlled conditions. A model for three wave-interference provides a better fit to the spectrum of the cavities, the calculated dimensions of the cavity also converged the direct microscope measurements.

5 Final Remarks and Future Work

The scope of this work was to explore the application of the PVDF in the optical sensing area. Firstly, an investigation was made in order to better understand the polymer behavior as a material. The most electroactive phase of PVDF was the focus of the study, due to its importance to the sensing technologies. Various methods for achieving the required phase were presented, being the solvent casting from DMF the chosen method for obtaining the PVDF in the β and γ phases. The samples were obtained by the dip coating technique with a 20%wt PVDF/DMF solution, the drying time was of two hours at ambient temperature for both thin films and SMF, or at 70 ºC for the thin films

The produced samples where characterized by XRD, DSC and FTIR-ATR. The FTIR-ATR revealed to be the more unveiling method to successfully characterize and distinguish the PVDF phases, since it allows to measure thin films and optical fiber. For the analysis of the XRD, only the thin films were able to be interpreted for PVDF, and for the DSC, even with a visible phase transition occurring, the interpretation of results was not as straightforward as the FTIR.

The thin films resulted in the expected presence of mainly γ-phase and some β-phase. For the optical fibers, a greater quantity of PVDF in the β-phase was observed, compared to the thin films. The SMF also have the presence of γ-phase. These two phases are electroactive and may be suitable for the application of the inverse piezoelectric effect. The relative quantity of the most electroactive phase, the β-phase, is also higher for the coated SMF, possibly due to the cylindrical geometry of the fibers.

The use of PVDF as a sensing element for an optical device was the focus of this work. Fabry-Perot interferometric cavities were produced relying on two and three wave interference. The dip coating technique was successfully used to deposit the polymer in the tip of the fiber. The fabrication process needs to be carefully controlled in order to have better results in the quality of the thin film, and to avoid deposition of PVDF in the lateral part of the fiber. In order to perform the controlled coating, a microscope stand was used to allow precise vertical adjustment for the dip.

The intrinsic FP may be interesting to analyze, but due to its large free spectral range, a broader source for characterization is needed. The cavities with the hollow tube are sensitive to humidity, with a maximum sensitivity of $39.28\,\mathrm{pm/\%RH}$, but the temperature sensitivity of these cavities is greater with a maximum sensitivity of $137\,\mathrm{pm/K}$.

A fine tuning of the optimal cavity parameters needs to be done. The variations in the temperature sensitivity may be caused by the three-wave interference, that have a more complex analysis than a simpler two-wave interference. The applied model for multiple wave interference – three-wave interference – was able to provide a better fit to the experimental spectra and confirm the microscope measurements.

Further investigation in this topic may still be done. Considering the results of the developed work, some of the possible cases of study are:

- Modeling the hollow-tube cavity to predict the behavior of the cavity considering different dimensions of the elements;
- Perform more controlled tests to be able to fully characterize the sensors;
- Optimize the length of the humidity sensor cavity;
- Explore the use of PVDF in other configurations for optical sensors, using for example, tapered fiber;
- Develop an electric field sensor using the PVDF as an actuator (see Appendix D).

References

[1] Y. Liu, B. Wang, Q. Zhan, Z. Tang, H. Yang, G. Liu, Z. Zuo, X. Zhang, Y. Xie, X. Zhu, B. Chen, J. Wang, R.-W. Li, Positive temperature coefficient of magnetic anisotropy in polyvinylidene fluoride (PVDF)-based magnetic composites, Sci. Rep. 4 (2014) 6615. doi:10.1038/srep06615.

[2] J. Tichy, J. Erhart, E. Kittinger, J. Privratska, Fundamentals of piezoelectric sensorics, Springer-Verlag Berlin Heidelberg, 2010. doi:10.1007/978-3-540-68427-5.

[3] H. Teng, Overview of the Development of the Fluoropolymer Industry, Appl. Sci. 2 (2012) 496–512. doi:10.3390/app2020496.

[4] P. Martins, A.C. Lopes, S. Lanceros-Mendez, Electroactive phases of poly(vinylidene fluoride): Determination, processing and applications, Prog. Polym. Sci. 39 (2014) 683–706. doi:10.1016/j.progpolymsci.2013.07.006.

[5] H.S. Nalwa, Ferroelectric Polymers: Chemistry, Physics, and applications, 1995.

[6] B. Ellis, R. Smith, eds., Polymers, A property database, 2nd ed., CRC Press, 2008.

[7] M. Imai, H. Tanizawa, Y. Ohtsuka, Y. Takase, A. Odajima, Piezoelectric copolymer jacketed single-mode fibers for electric-field sensor application, J. Appl. Phys. 60 (1986) 1916. doi:10.1063/1.337242.

[8] S.B. Lang, S. Muensit, Review of some lesser-known applications of piezoelectric and pyroelectric polymers, Appl. Phys. A Mater. Sci. Process. 85 (2006) 125–134. doi:10.1007/s00339-006-3688-8.

[9] B. Fay, G. Ludwig, C. Lankjaer, P.A. Lewin, Frequency response of PVDF needle-type hydrophones, Ultrasound Med. Biol. 20 (1994) 361–366. doi:10.1016/0301-5629(94)90004-3.

[10] P.C. Beard, T.N. Mills, Extrinsic optical-fiber ultrasound sensor using a thin polymer film as a low-finesse Fabry-Perot interferometer., Appl. Opt. 35 (1996) 663–675. doi:10.1364/AO.35.000663.

[11] A. V. Shirinov, W.K. Schomburg, Pressure sensor from a PVDF film, Sensors Actuators, A Phys. 142 (2008) 48–55. doi:10.1016/j.sna.2007.04.002.

[12] H.D. Wiederick, J. a. Rody, R.J. Stockermans, B.K. Mukherjee, A pyroelectric

PVdF temperature sensor for cryogenic temperatures, [Proceedings] 1990 IEEE 7th Int. Symp. Appl. Ferroelectr. (1990) 387. doi:10.1109/ISAF.1990.200268.

[13] Y.F. Jia, Q.S. Ni, X.J. Chen, C. Ju, K.L. Xing, T.H. Jin, Simulation and Experiment of PVDF Temperature Sensor, Appl. Mech. Mater. 303–306 (2013) 109–113. doi:10.4028/www.scientific.net/AMM.303-306.109.

[14] A. Odon, Probe with PVDF Sensor for Energy Measurements of Optical Radiation, Meas. Sci. Rev. 3 (2003) 111–114.

[15] J.S. Lee, K. Shin, O.J. Cheong, J.H. Kim, J. Jang, Highly Sensitive and Multifunctional Tactile Sensor Using Free-standing ZnO / PVDF Thin Film with Graphene Electrodes for Pressure and Temperature Monitoring, Sci. Rep. 5 (2015) 1–8. doi:10.1038/srep07887.

[16] 0.2mm Probe, Precis. Acoust. (n.d.). http://acoustics.co.uk/products/pressure-intensity-measurements/needle-hydrophones/0-2mm-probe/ (accessed February 1, 2016).

[17] J.M. Corres, J. Ascorbe, F.J. Arregui, I.R. Matias, Tunable electro-optic wavelength filter based on lossy-guided mode resonances, Opt. Express. 21 (2013) 31668–31677. doi:10.1364/OE.21.031668.

[18] J. Ascorbe, J.M. Corres, I.R. Matias, F.J. Arregui, Optical fiber current transducer using lossy mode resonances for high voltage networks, 9157 (2014) 91578S. doi:10.1117/12.2059629.

[19] J.M. Corres, Y.R. Garcia, F.J. Arregui, I.R. Matias, Optical fiber humidity sensors using PVdF electrospun nanowebs, IEEE Sens. J. 11 (2011) 2383–2387. doi:10.1109/JSEN.2011.2123881.

[20] S. Muto, O. Suzuki, T. Amano, M. Morisawa, A plastic optical fibre sensor for real-time humidity monitoring, Meas. Sci. Technol. 14 (2003) 746–750. doi:10.1088/0957-0233/14/6/306.

[21] R. Grecorio, M. Cestari, Effect of Crystallization Temperature on the Crystalline Phase Content and Morphology of Poly (vinylidene Fluoride), J. Polym. Sci. Part B Polym. Phys. Vol. 32 (1994) 859–870. doi:10.1002/polb.1994.090320509.

[22] R. Gregorio, D.S. Borges, Effect of crystallization rate on the formation of the polymorphs of solution cast poly(vinylidene fluoride), Polymer (Guildf). 49 (2008) 4009–4016. doi:10.1016/j.polymer.2008.07.010.

[23] D.L. Chinaglia, R. Gregorio, J.C. Stefanello, R.A.P. Altafim, W. Wirges, F. Wang, R. Gerhard, Influence of the solvent evaporation rate on the crystalline phases of solution-cast poly(vinylidene fluoride) films, J. Appl. Polym. Sci. 116 (2010) 785–791. doi:10.1002/app.31488.

[24] W. Steinmann, S. Walter, M. Beckers, G. Seide, T. Gries, Thermal Analysis of Phase Transitions and Crystallization in Polymeric Fibers, Appl. Calorim. a Wide Context - Differ. Scanning Calorimetry, Isothermal Titration Calorim. Microcalorim. (2013). doi:10.5772/54063.

[25] R. Gregorio, Determination of the α, β, and γ crystalline phases of poly(vinylidene fluoride) films prepared at different conditions, J. Appl. Polym. Sci. 100 (2006) 3272–3279. doi:10.1002/app.23137.

[26] A. Salimi, A.A. Yousefi, FTIR studies of β-phase crystal formation in stretched PVDF films, Polym. Test. 22 (2003) 699–704. doi:10.1016/S0142-9418(03)00003-5.

[27] J. Liu, X. Lu, C. Wu, Effect of preparation methods on crystallization behavior and tensile strength of poly(vinylidene fluoride) membranes, Membranes (Basel). 3 (2013) 389–405. doi:10.3390/membranes3040389.

[28] G. Laroche, C.P. Lafrance, R.E. Prud'homme, R. Guidoin, Identification and quantification of the crystalline structures of poly(vinylidene fluoride) sutures by wide-angle X-ray scattering and differential scanning calorimetry, J Biomed Mater Res. 39 (1998) 184–189. http://www.ncbi.nlm.nih.gov/htbin-post/Entrez/query?db=m&form=6&dopt=r&uid=0009457546.

[29] G.T. Davis, J.E. McKinney, M.G. Broadhurst, S.C. Roth, Electric-field-induced phase changes in poly(vinylidene fluoride), J. Appl. Phys. 49 (1978) 4998–5002. doi:10.1063/1.324446.

[30] X.I. Yingxue, F.A.N. Huiqing, L.I.U. Weiguo, Y. Chen, N.I.U. Xiaoling, A STUDY ON THERMO-OPTIC EFFECT OF β POLY (VINYLIDENE FLUORIDE) THIN FILMS PREPARED BY SOLUTION CASTING METHOD, 15 (2008) 175–181.

[31] D.R. Dillon, K.K. Tenneti, C.Y. Li, F.K. Ko, I. Sics, B.S. Hsiao, On the structure and morphology of polyvinylidene fluoride-nanoclay nanocomposites, Polymer (Guildf). 47 (2006) 1678–1688. doi:10.1016/j.polymer.2006.01.015.

[32] Y. Bormashenko, R. Pogreb, O. Stanevsky, E. Bormashenko, Vibrational

spectrum of PVDF and its interpretation, Polym. Test. 23 (2004) 791–796. doi:10.1016/j.polymertesting.2004.04.001.

[33] M. Benz, W.B. Euler, Determination of the crystalline phases of poly(vinylidene fluoride) under different preparation conditions using differential scanning calorimetry and infrared spectroscopy, J. Appl. Polym. Sci. 89 (2003) 1093–1100. doi:10.1002/app.12267.

[34] P. Morris, A. Hurrell, A. Shaw, E. Zhang, P. Beard, A Fabry–Pérot fiber-optic ultrasonic hydrophone for the simultaneous measurement of temperature and acoustic pressure, J. Acoust. Soc. Am. 125 (2009) 3611. doi:10.1121/1.3117437.

[35] H. Van De Stadt, J.M. Muller, Multimirror Fabry-Perot interferometers, J. Opt. Soc. Am. A. 2 (1985).

Appendix A PVDF/DMF preparation protocol

In order to prepare the PVDF/DMF solution the following detailed laboratorial protocol was followed. In this example, final solution has a concentration of 20 (%wt).

1. Turn on the hotte's light and extraction;
2. Place the magnetic stirrer with hotplate in the hotte;
3. Prepare an amber glass container (flask);
    a. Place the stirring magnet inside the flask;
    b. Weight 2 grams of PVDF and place it inside the flask;
4. Using another container, measure 10 mL of DMF;
    a. If the DMF is not available in a medium/small container, an intermediate medium container should be prepared beforehand to prevent accidents during this step;
    b. Add the 10 mL of DMF to the flask with PVDF;
5. Seal the flask to prevent volatile DMF vapors to escape, Parafilm can be used;
6. Place the flask on the hotplate over a silicone base, if possible;
    a. Set the hotplate to 40ºC and the stirrer to 700 rpm;
    b. The temperature and rotation speed values can be adjusted using the mixing process;
    c. This step takes about 1h30m, it varies for each solution;
7. Turn off the hotplate and the stirrer;
8. Store the sealed flask in a low light
9. Wash, dry and store the material;
10. Turn off the hotte's light and extraction;

Appendix B GPIB communication protocol

The data acquisition in the Temperature and Humidity tests needed to be automated due to the restrictions both in the OSA and in the experimental setup's room. ANDO's OSAs features the possibility of being automated by writing a code directly in the OSA. The time synchronization is one of the problems with the OSA's own program, the time between the begin of two measurements can't be programed. The OSA can only be coded with waiting times between two tasks (ie. saving the data and performing a measurement). Also, two different measurements can also have different duration. Altogether, the sync between the climatic chamber and the measurement setup can be a problem. The alternative was to code a LabView routine to have direct control of the OSA. With this alternative one can run the experience in the climatic chamber not worrying too much with syncing, the number of sample points per measurement, nor the data storage.

The communication protocol used was the GPIB, which the OSA6331 has available. The form of the GPIB Orders, Query, and Responses for the OSA6331 were consulted in the manual of the equipment. The VI for a general Query routine is presented in the Figure B-1. This VI waits for the START button to be pressed and after being pressed, it first opens the GPIB session between the selected equipment and LabView, then, the custom Command (Query or Order) is written to the buffer and sent to the OSA. If the Command is a Query, the OSA sends a Response, that is read and stored in the read buffer. The next step, Clearing the Buffer, is not essential but assures that the Read Buffer is empty and if any information is there, it won't interfere with future communications. The last step the VI performs is closing the GPIB session.

This VI was used as base for various sub-VI that automatically perform various Commands or Queries, returning the OSA's response String to LabView. The use of sub-Vis lets more complex programing to be implemented by the user in a quicker and easier way.

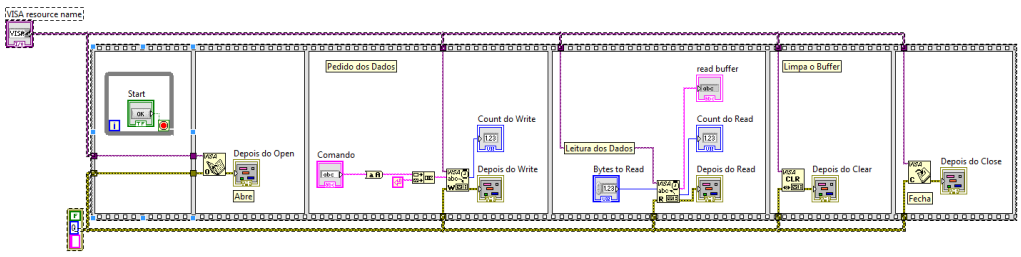

Figure B-1 – Customizable sub-VI used to code simple Commands/Queries

B.1 Routine Read/Wait/internal Save

The simplest routine that was programed is presented in the Figure B-2, this routine performs a “SINGLE” sweep measurement, waits for the measurement to end and then, if desired, saves the data to the floppy disk.

The wait function Queries the OSA6331 multiple times until the answer signals that the equipment ended the single sweep. More recent equipment would not require this kind of wait function because the instruments have alternate ways to signal the end of the single sweep. Nonetheless, more recent drivers for other Yokogawa (formerly ANDO) OSAs still use a similar way of verifying if the OSA has ended the sweep operation.

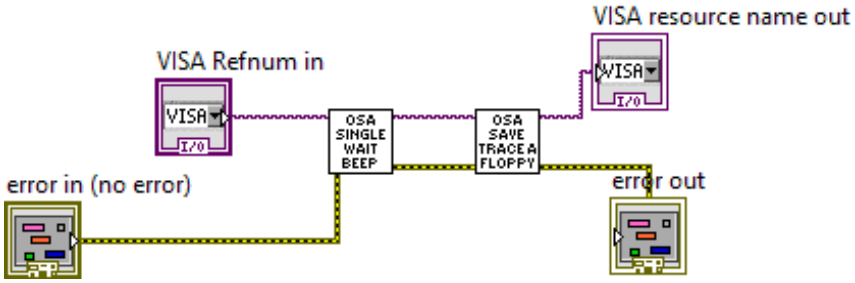

Figure B-2 – Read / Wait / internal Save routine

B.2 Acquire (DUMP) Trace

The Acquire Trace routine, in the Figure B-3, provides a way for the user to directly obtain the experimental data without using the floppy disk. This routine asks the OSA to send the selected TRACE data. Depending on the sample points (maximum of 5001 points for the OSA6331), the 6331 will begin to write on the buffer, which the LabView will read and store in a local variable to be processed.

When reading the buffer, if the user or LabView doesn’t assert the correct number of bytes expected, the program may eventually run into an error. With the help of the 6331’s manual, the string’s arrangements were consulted and the exact number of bytes that is generated for each sampling was determined. Some mathematical operations were implemented in order to automatically determine this number and feed it to the VI.

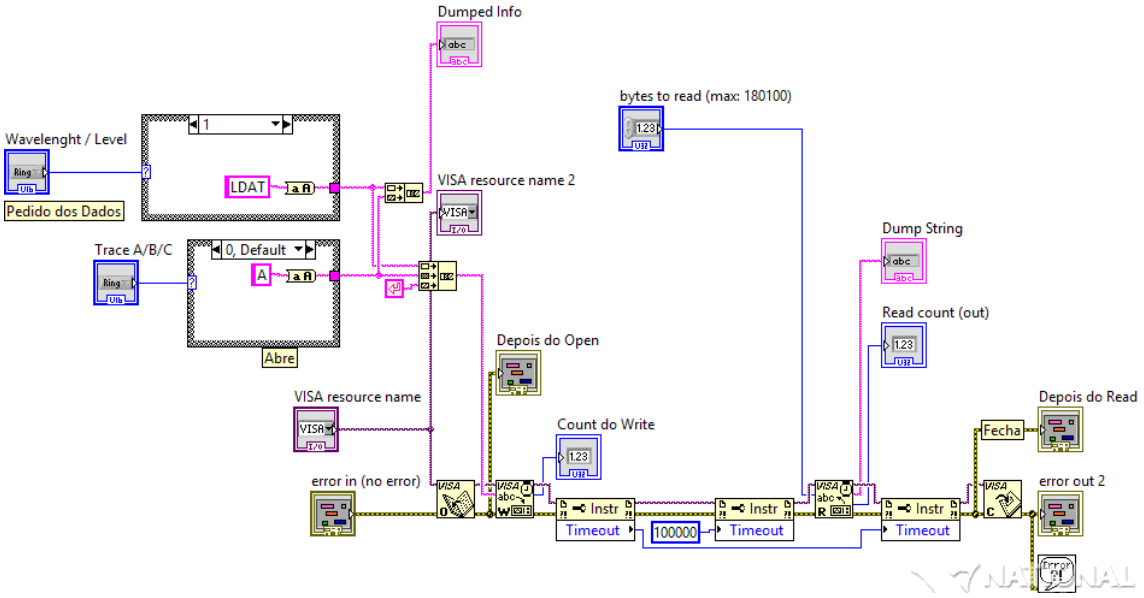

Figure B-3 – Acquire (DUMP) Trace routine

B.3 Save Acquired Trace in a text file

In order to have a user-friendly file to analyze after the experiment, this LabView routine reorganizes the experimental data from a one-line string into a table with two columns. Depending on this VI's version, it also stores some useful information as the time and date of the measurement, number of sample points, sensitivity, among other properties. The VI can be directly fed with the output string stored after the TRACE DUMP from the OSA6331 or with a similar one-line text file loaded from the computer. The conversion's block diagram is depicted in the Figure B-4 and the saving process is presented in the Figure B-5.

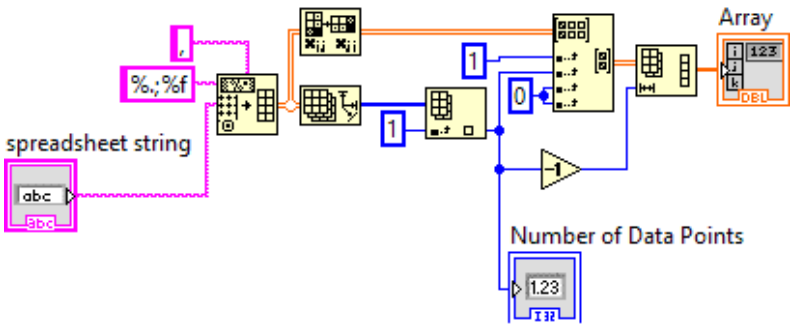

Figure B-4 - Convert routine

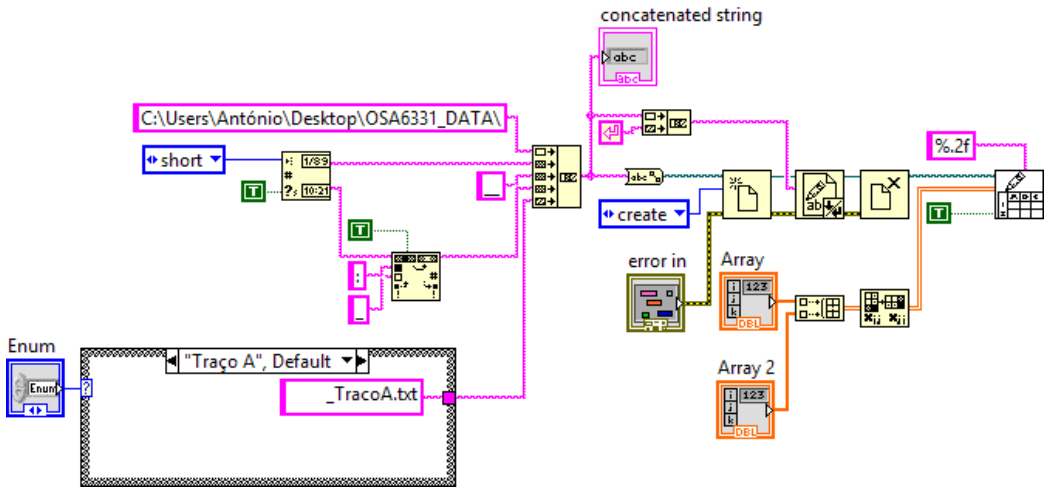

Figure B-5 – Save file routine

B.4 Read/Dump/Save/Wait

The Read/Dump/Save/Wait routine is the timed VI that was used in during the experiment, it performs the described actions. First it sends a Command for the OSA to perform a SINGLE sweep, then it Queries the OSA to retrieve the measured data. After this, the routine processes the data and stores it in the computer. Meanwhile, a timer was set from the beginning of the SINGLE sweep, if the time delay is set to 15 minutes, each sweep will be performed with intervals of 15 minutes. This routine starts running only after a button is pressed, and it only stops after a STOP button is hit. The block diagram for this VI is depicted in the Figure B-6.

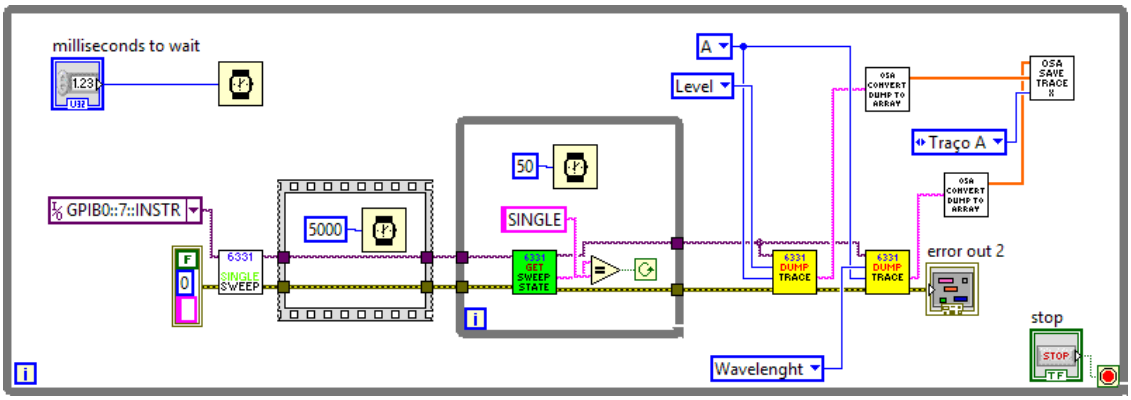

Figure B-6 – Read/Dump/Save/Wait timed routine

Appendix C Model for the PVDF Fabry-Perot cavity

Considering a three wave approach to the optical cavity, a third reflection needs to be taken in consideration. As presented in the Figure C-1, there are three reflected beams: the first, in the interface between the SMF's silica core, and the air, with reflection coefficient R_1; the second reflection occurs in the first interface between the air and the PVDF and has a reflection coefficient of R_2; the third reflection, with coefficient R_3, occurs in the last interface between the PVDF and the air.

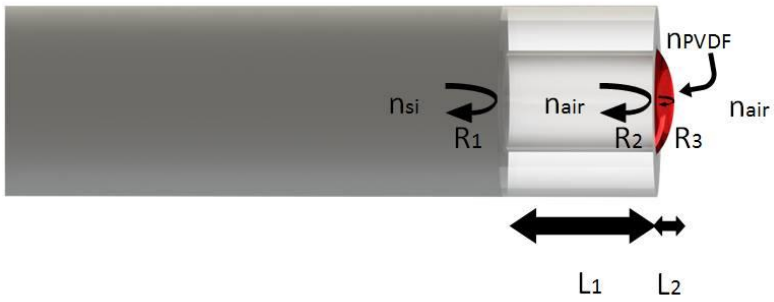

Figure C-1 - Diagram for the Fabry-Perot with a three wave approach

The equation (1a) shows the transmitted intensity for the cavity parameters [35]. The reflection coefficients, r_i, can be calculated from the Fresnel equations for two media interfaces with different refraction indexes. The phases of the cosines are dependent from the lengths l_1 and l_2. This phase is given by the following equation, $\phi_i = \frac{2\pi * \mathrm{l}_i \mathrm{n}_i}{\lambda}$.

$$I_t(\lambda) = \frac{(1-r_1^2)(1-r_2^2)(1-r_3^2)}{1+B} \tag{1a}$$

$$\begin{aligned} B = {} & (r_1 r_2)^2 + (r_2 r_3)^2 + (r_1 r_3)^2 + 2r_1 r_2 (1-r_3^2)\cos[2\phi_1] \\ & + 2r_2 r_3 (1-r_1^2)\cos[2\phi_1] + 2r_1 r_3 \cos[2\phi_1 + 2\phi_2] \\ & + 2r_1 r_2^2 r_3 \cos[2\phi_1 - 2\phi_2] \end{aligned} \tag{2b}$$

The model was used to fit the measured spectra as presented in the Section 4.3.

Using the termo-optic effect and the coefficient of expansion for the PVDF for varying the parameters of a given cavity, the behavior of the sensor was verified.

Appendix D Electrical Sensor Design

A sensor configuration for electrical current sensing, based in the piezoelectric nature of PVDF, was developed. A similar sensor is proposed in the literature, but its principle is based in the LMR mechanism [17,18].

The sensor design and production steps is depicted in the Figure D-1. A Fabry-Perot cavity obtained by fusion splicing a silica hollow-tube between two SM fibers. Two metallic contacts are deposited in the sidewalls of the SMF to serve as electrodes. A thin film of electroactive PVDF is used to cover the cavity. The response of the PVDF to the electric current will be transduced to the cavity length variation, thus creating the electrical sensing device.

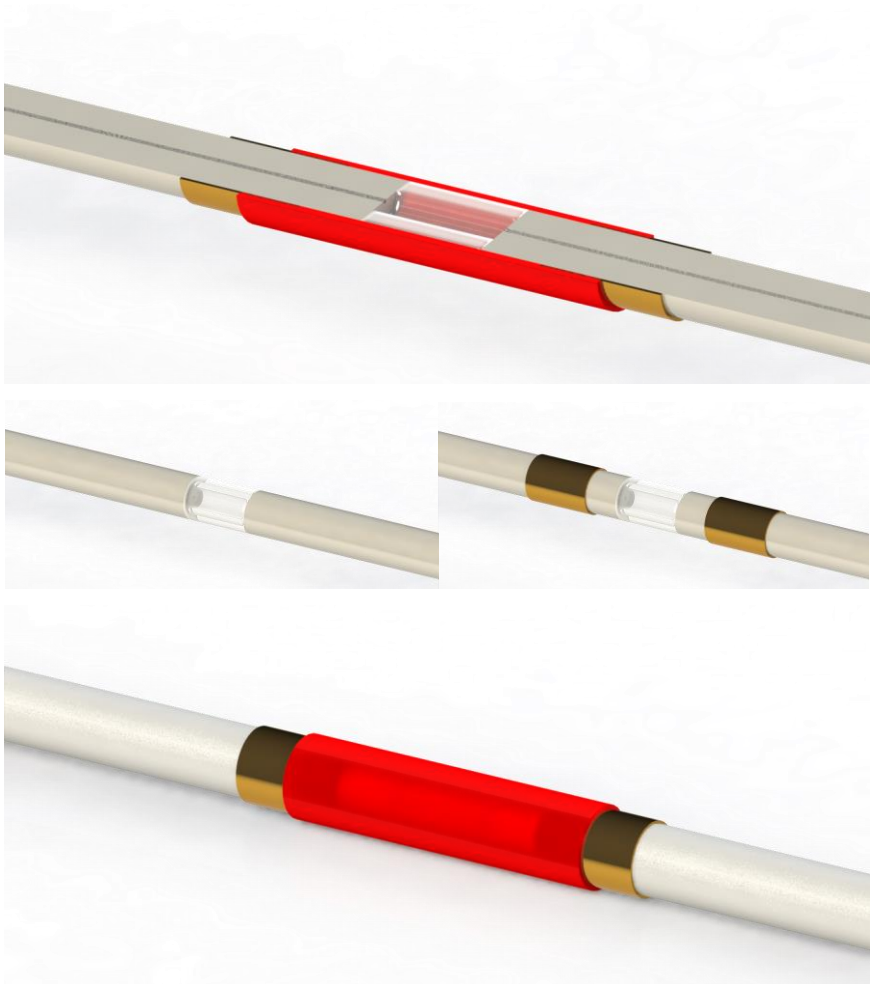

Figure D-1 – Design and Fabrication Process for a FP current sensor